Enhanced X-ray Emission Coinciding with Giant Radio Pulses from the Crab Pulsar

Teruaki Enoto (RIKEN, NICER M&M team)

Toshio Terasawa, Shota Kisaka, Chin-Ping Hu, Sebastien Guillot, Natalia Lewandowska, Christian Malacaria, Paul S. Ray, Wynn C.G. Ho, Alice K. Harding, Takashi Okajima, Zaven Arzoumanian, Keith C. Gendreau, Zorawar Wadiasingh, Craig B. Markwardt, Yang Soong, Steve Kenyon, Slavko Bogdanov, Walid A. Majid, Tolga Guver, Gaurava K. Jaisawal, Rick Foster, Yasuhiro Murata, Hiroshi Takeuchi, Kazuhiro Takefuji, Mamoru Sekido, Yoshinori Yonekura, Hiroaki Misawa, Fuminori Tsuchiya, Takahiko Aoki, Munetoshi Tokumaru, Mareki Honma, Osamu Kameya, Tomoaki Oyama, Katsuaki Asano, Shinpei Shibata and Shuta J. Tanaka

Enoto et al., Science, 372, 187-190 (2021) [arXiv: 2104.03492]

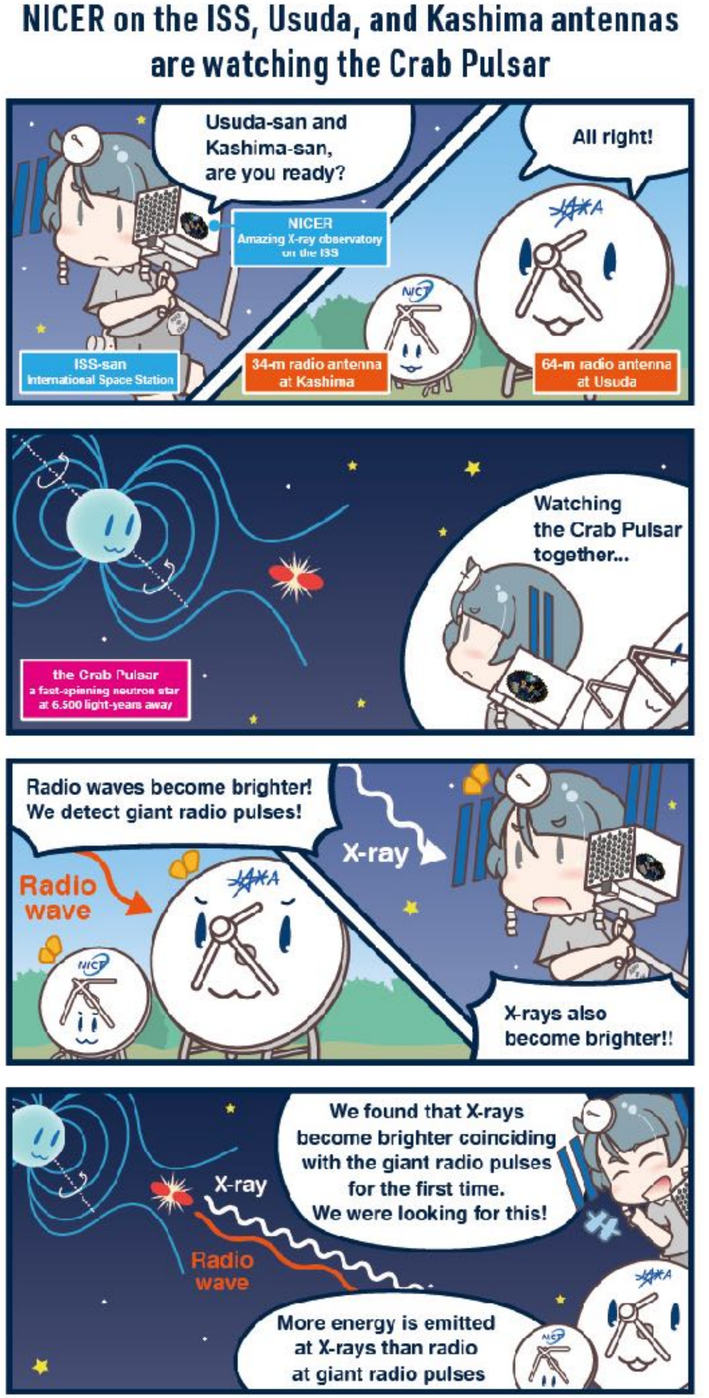

(Credig) Higgstan.com

中性子星の観測と理論〜研究活性化ワークショップ2021〜 @ 2021-08-10 ポスターセッション

A FRB was found from a Galactic magnetar!!

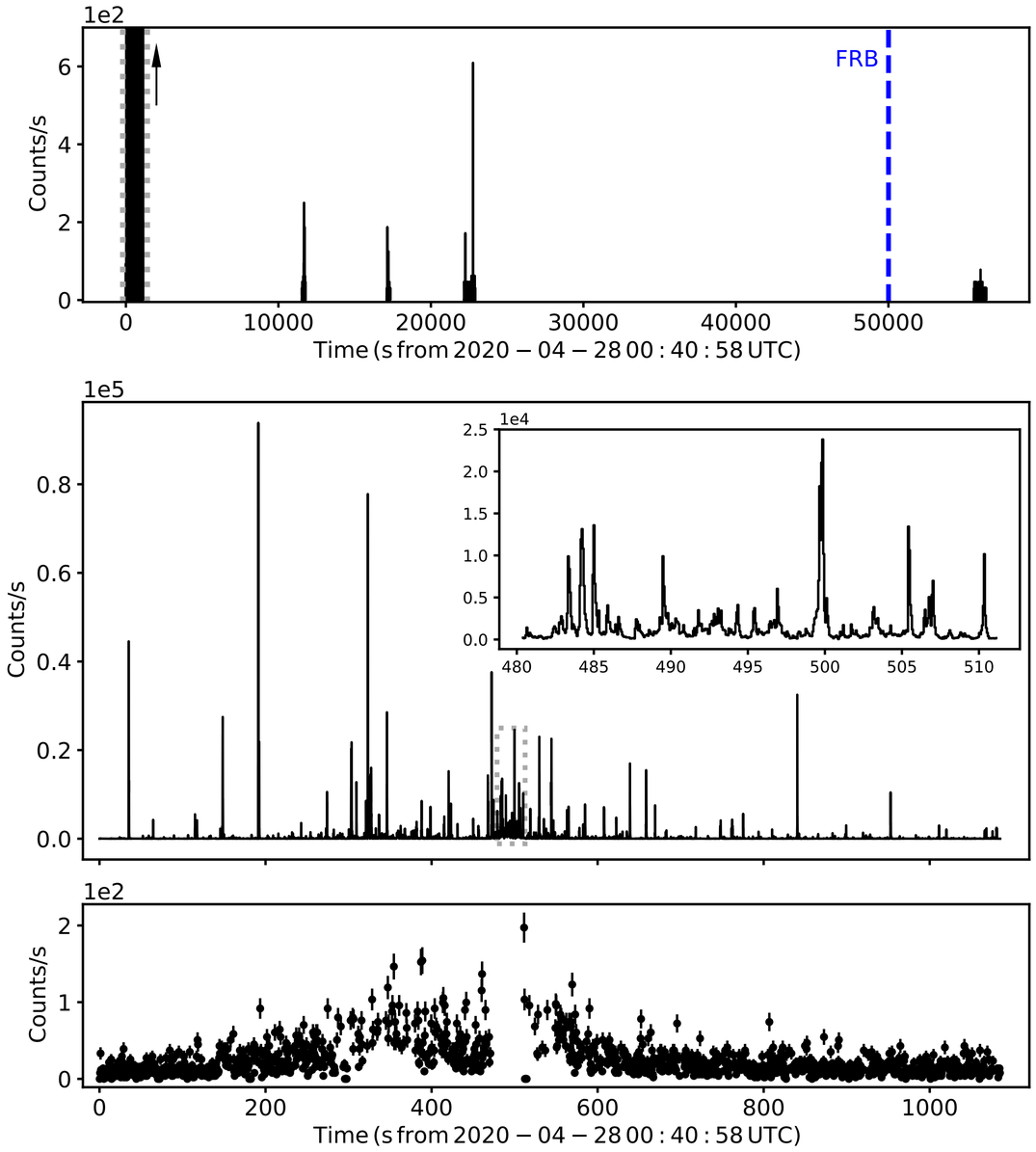

- Galactic magnetar SGR 1935+2154
  - discovered in 2014 (~9 kpc?)
  - P=3.24 s, Pdot=1.43e-11 s/s
  - B ~ 2.2e+14 G
- A burst was detected with Swift Burst Alert Telescope on April 27, 2020.
- X-ray follow-up monitoring by several X-ray observatories, including NICER.
- X-ray burst forest was found from the Galactic magnetar SGR 1935+2154 on 2020 April 28.
- A FRB was found during this activated state!

Younes et al., arXiv:2009.07886

A FRB was found from a Galactic magnetar!!

- Two-peak FRB coincided with a magnetar X-ray burst (Insight-HMXT, INTEGRAL, AGILE, and Konus-Wind)

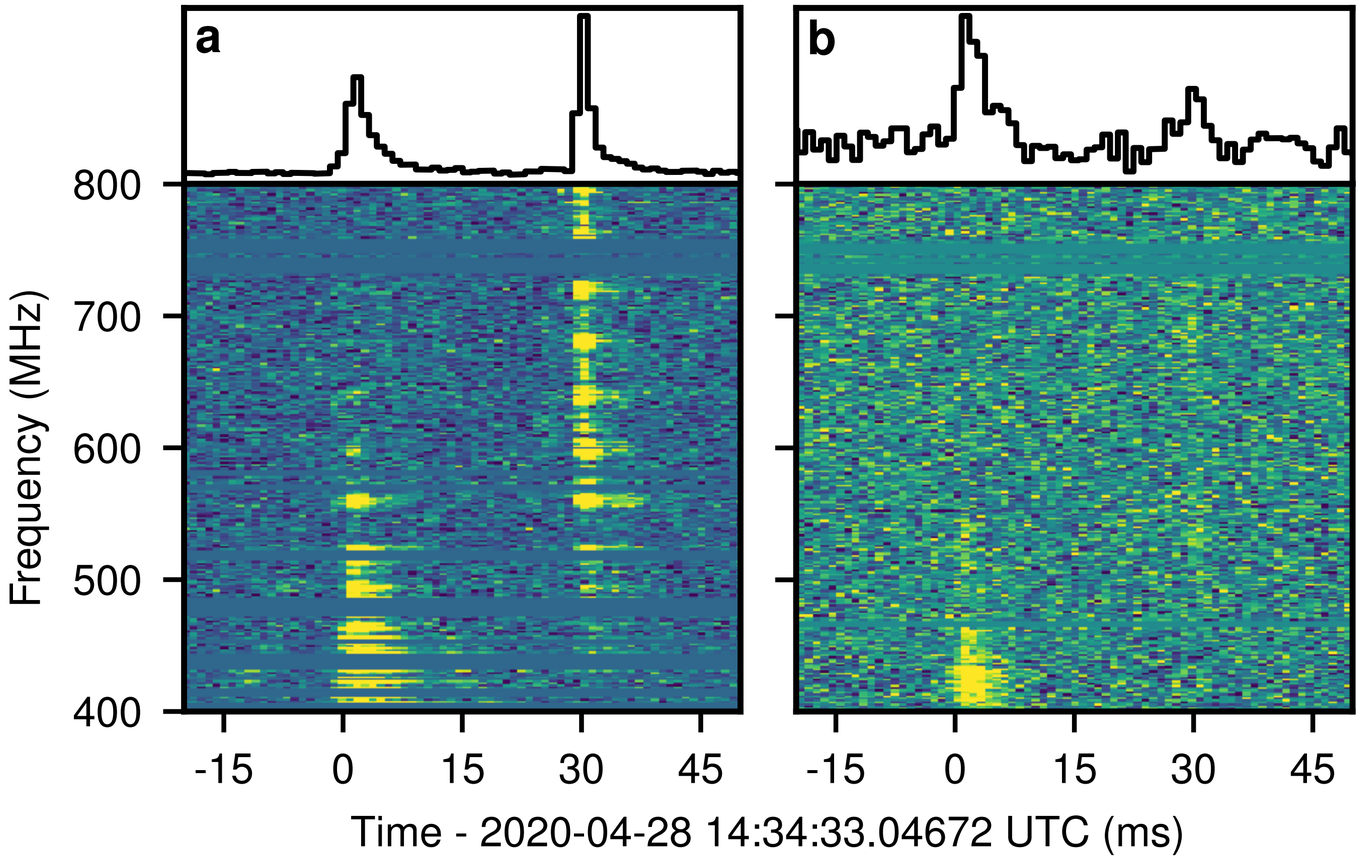

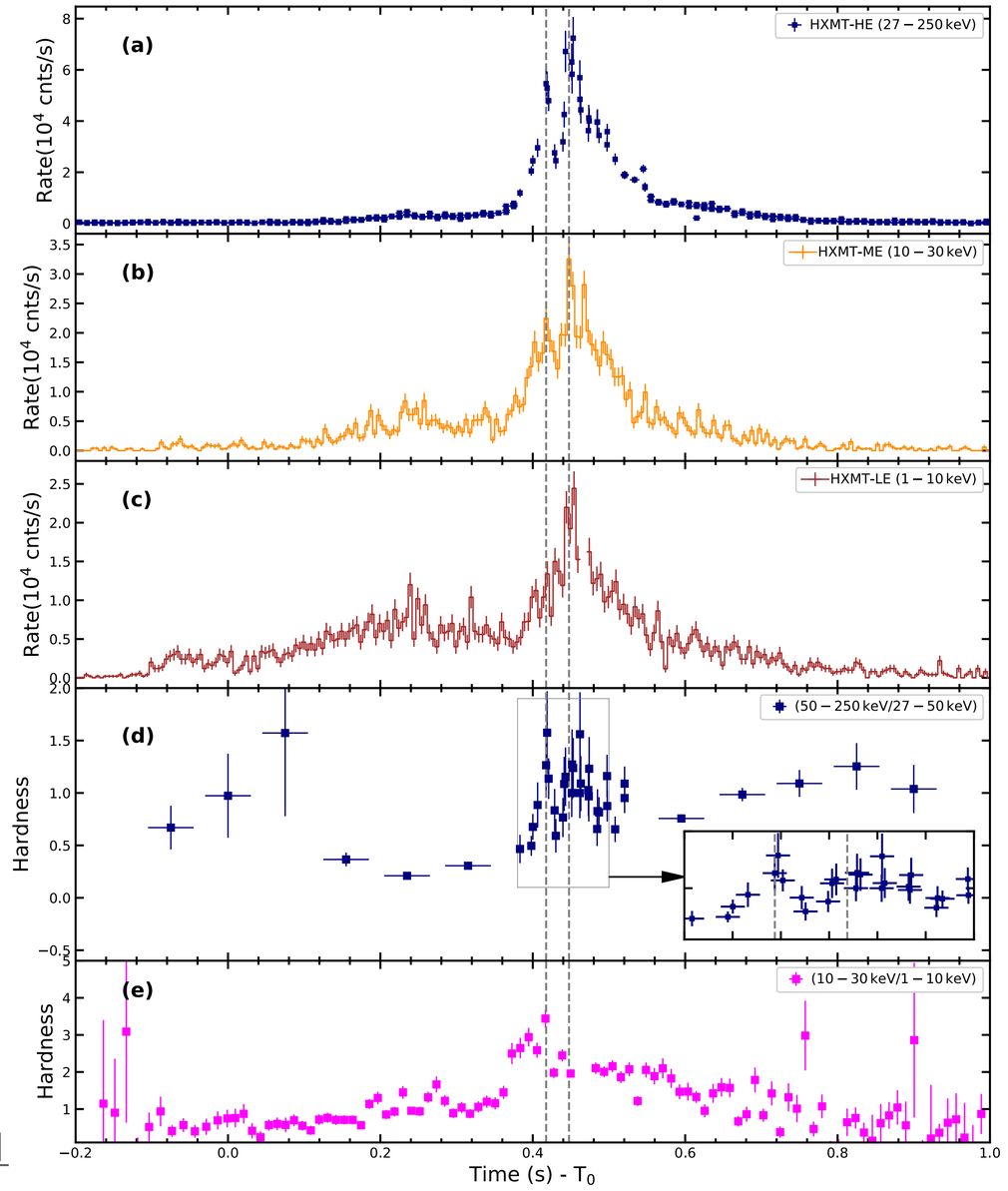

The CHIME/FRB Collaboration, arXiv:2005.10324

Li et al., arXiv 2005.11071

Galactic FRB vs. Cosmological FRBs

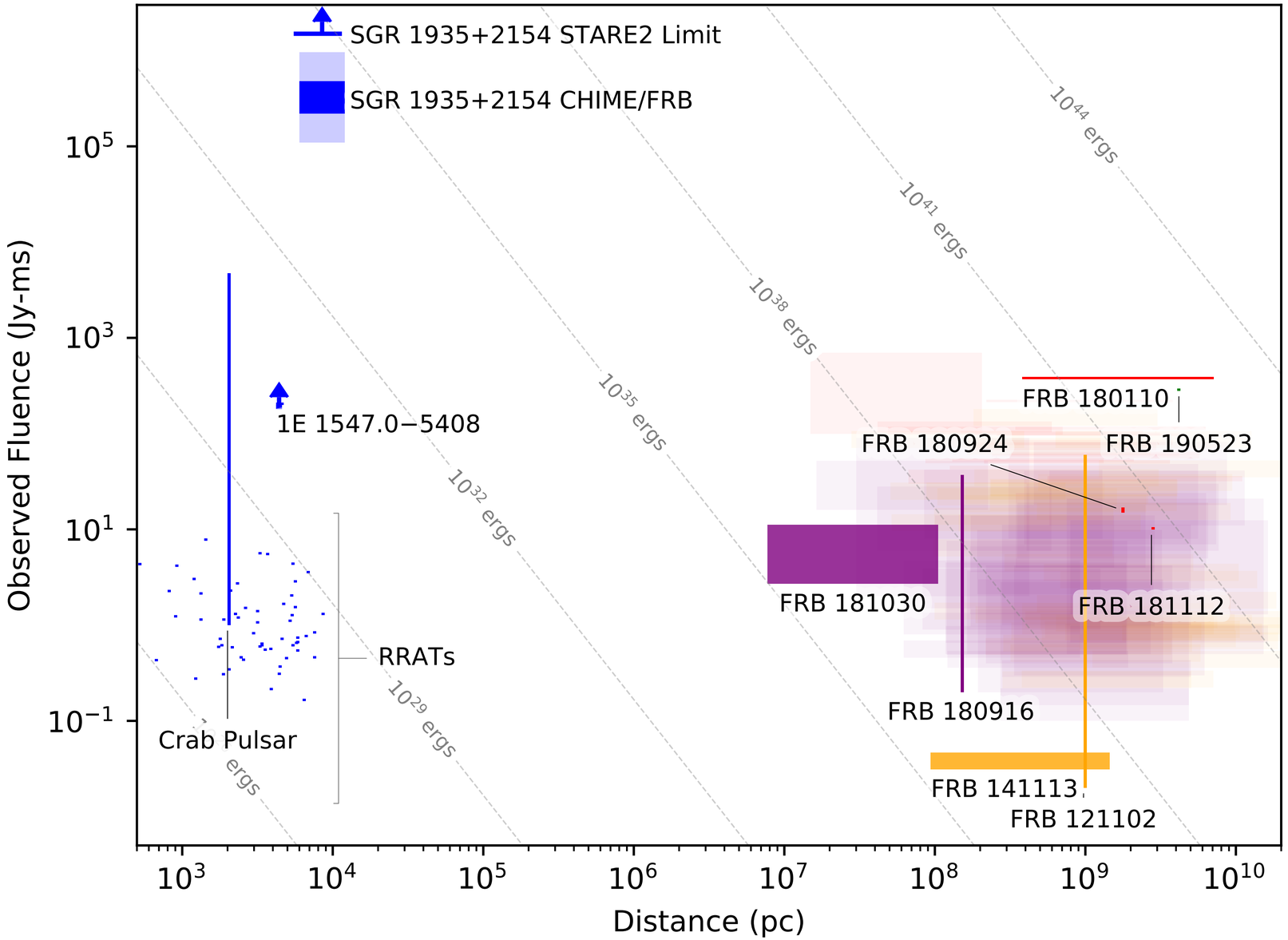

- Compared with extra-Galactic FRBs, this Galactic FRB is
  - Higher fluence
  - Lower luminosity
- Implication: FRB coherent (?) radio emission and incoherent X-ray burst are related with each other.

The CHIME/FRB Collaboration, arXiv:2005.10324

FRB-associated burst vs. Other magnetar bursts

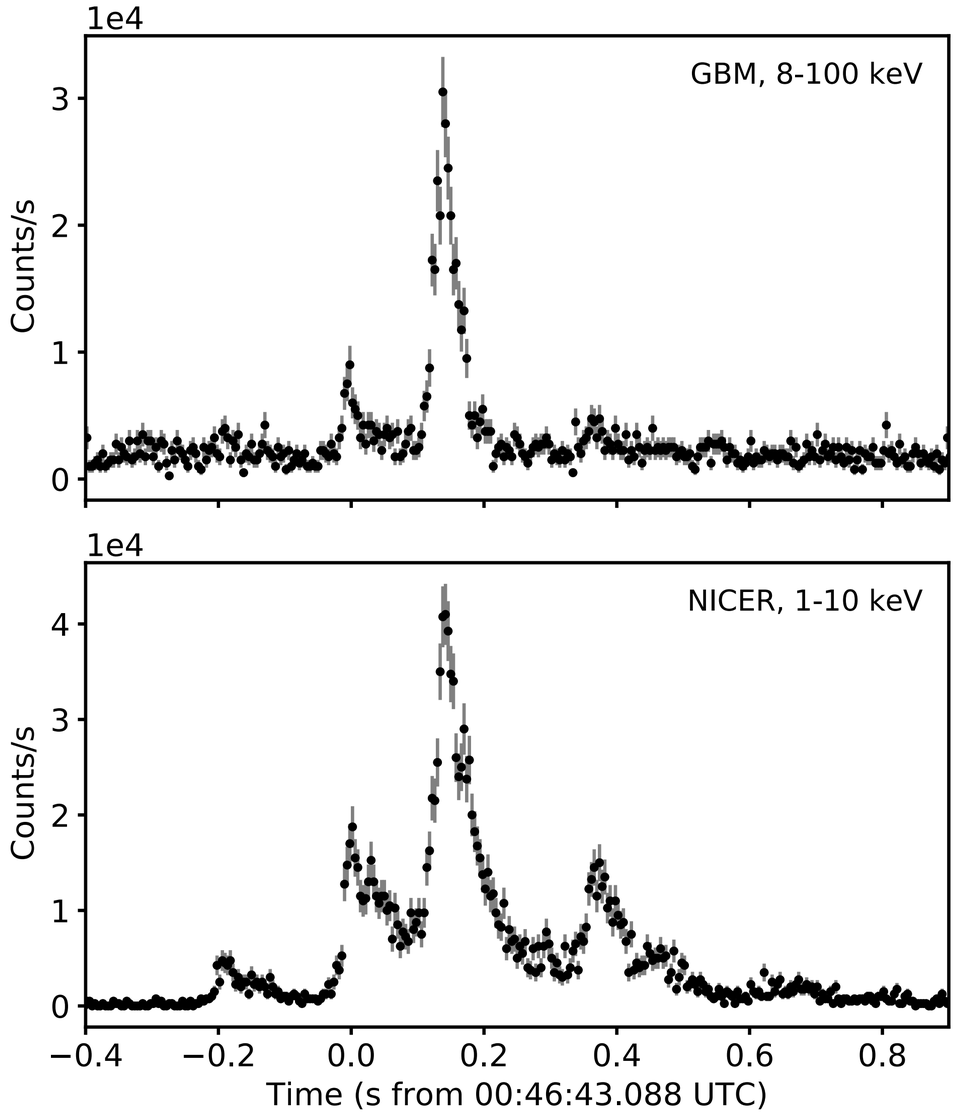

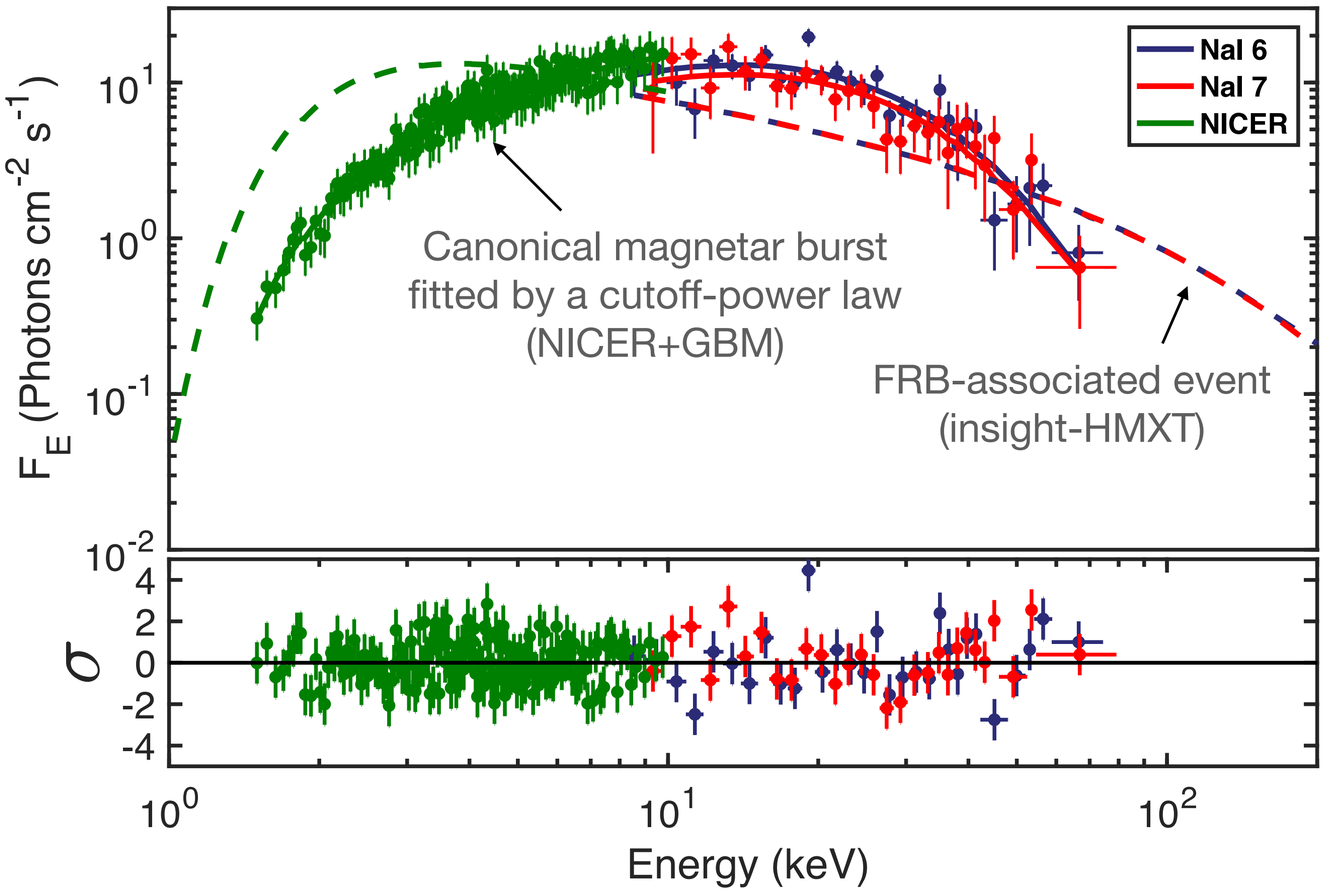

- Example of a magnetar short burst from SGR 1935+2154 observed with NICER+GBM compared with the FRB-associated event.

Younes et al.., arXiv: 200611358

X-ray burst spectrum: FRB-associated vs. others

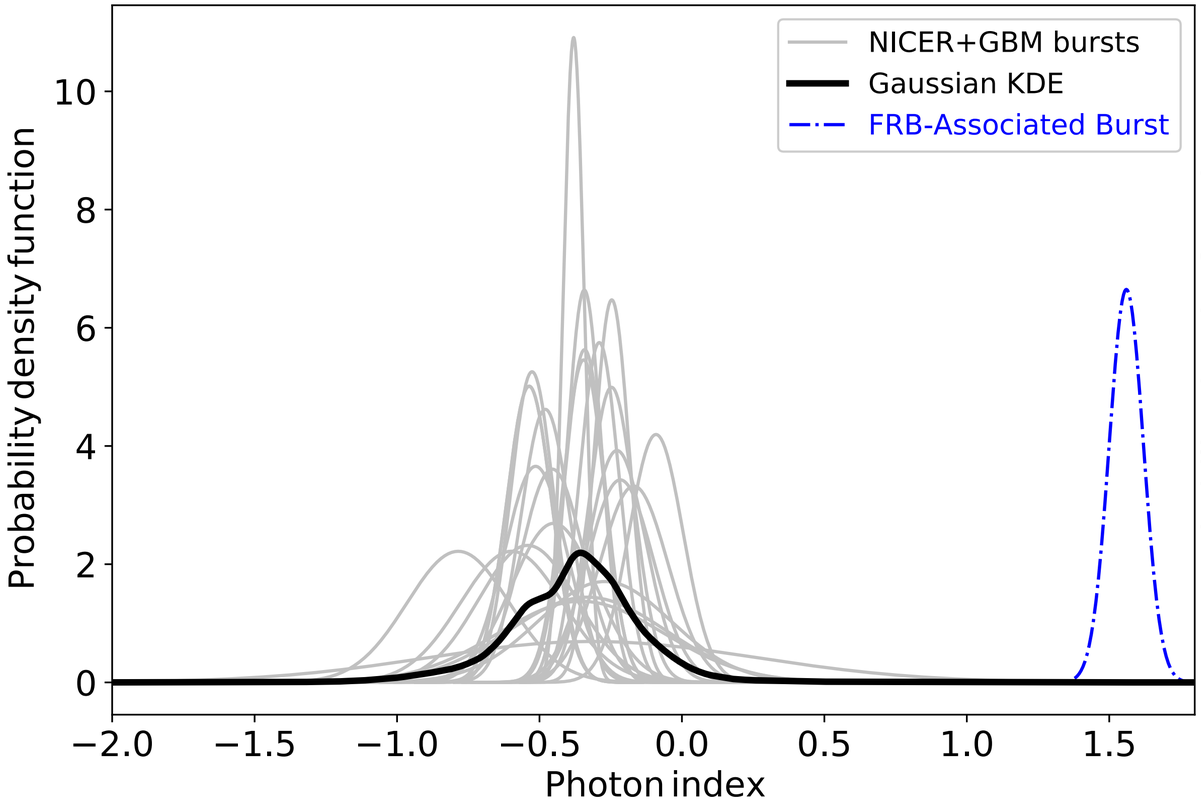

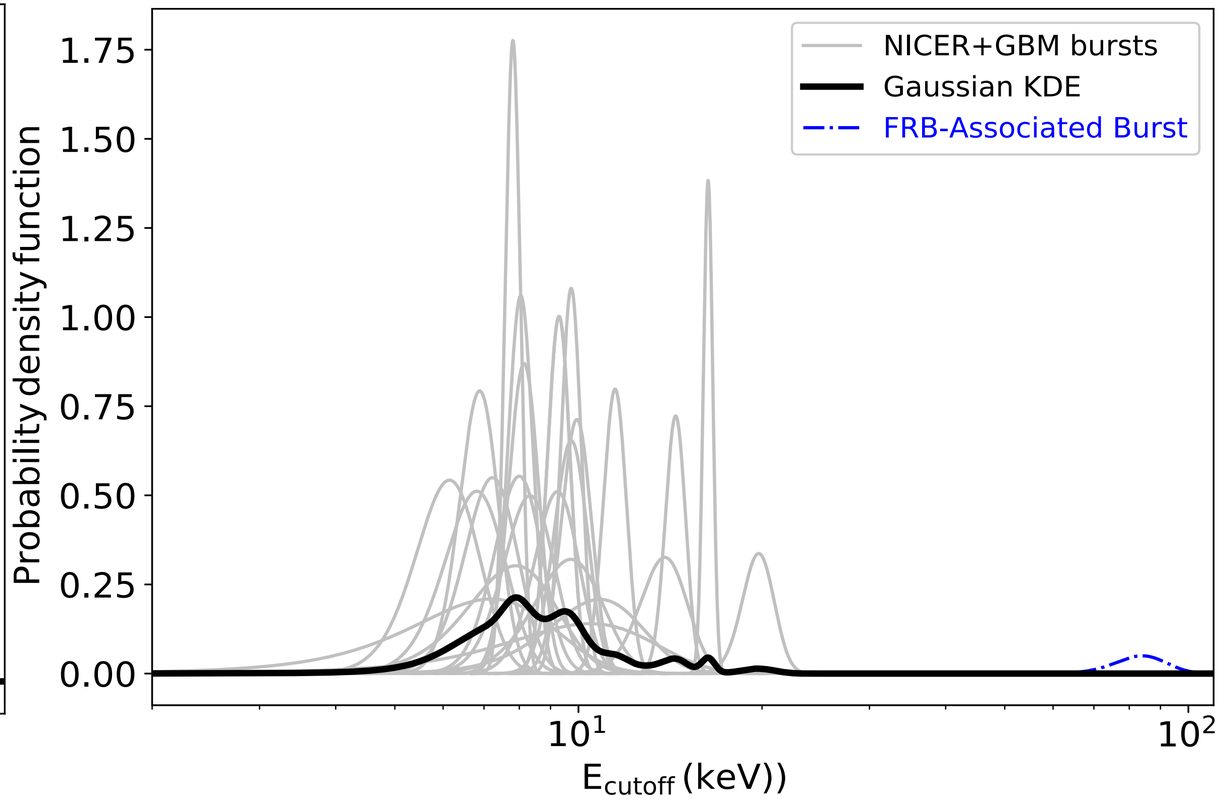

- Probability distribution function of X-ray spectral parameters of 24 short bursts from SGR 1935+2154: Cutoff power-law index (left) and cutoff energy (right).
- The FRB-associated burst is different from the other X-ray bursts?

Younes et al.., arXiv: 200611358

X-ray burst spectrum: FRB-associated vs. others

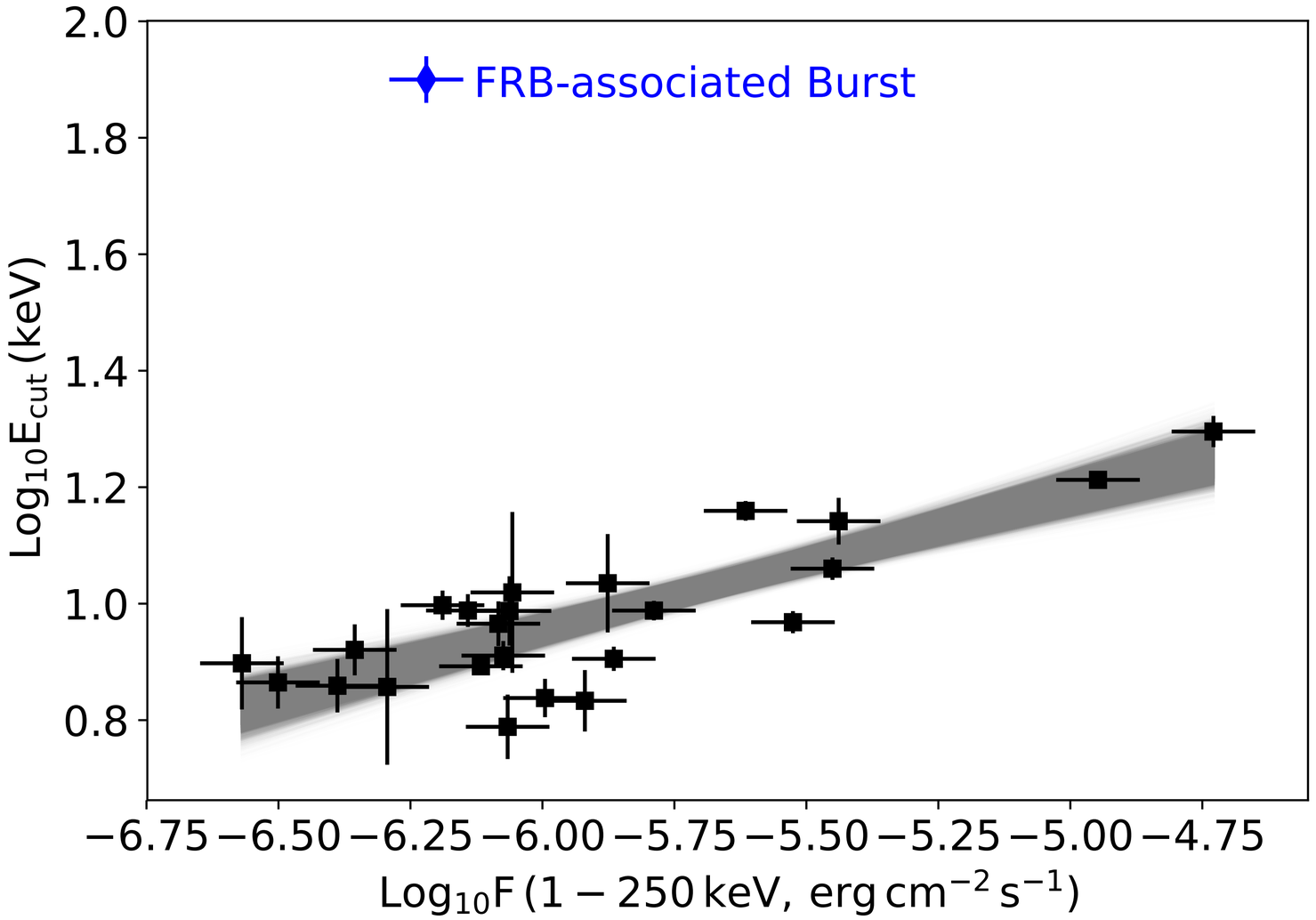

- Cutoff energy vs. X-ray flux in 1-250 keV.
- Brighter magnetar short burst shows higher cutoff energy.
- X-ray flux of the FRB-associated burst is in the distribution of the other (canonical) magnetar bursts.
- However, the cutoff energy of the FRB-associated one is higher than the others.

Younes et al.., arXiv: 200611358

Galactic FRB vs. Cosmological FRBs

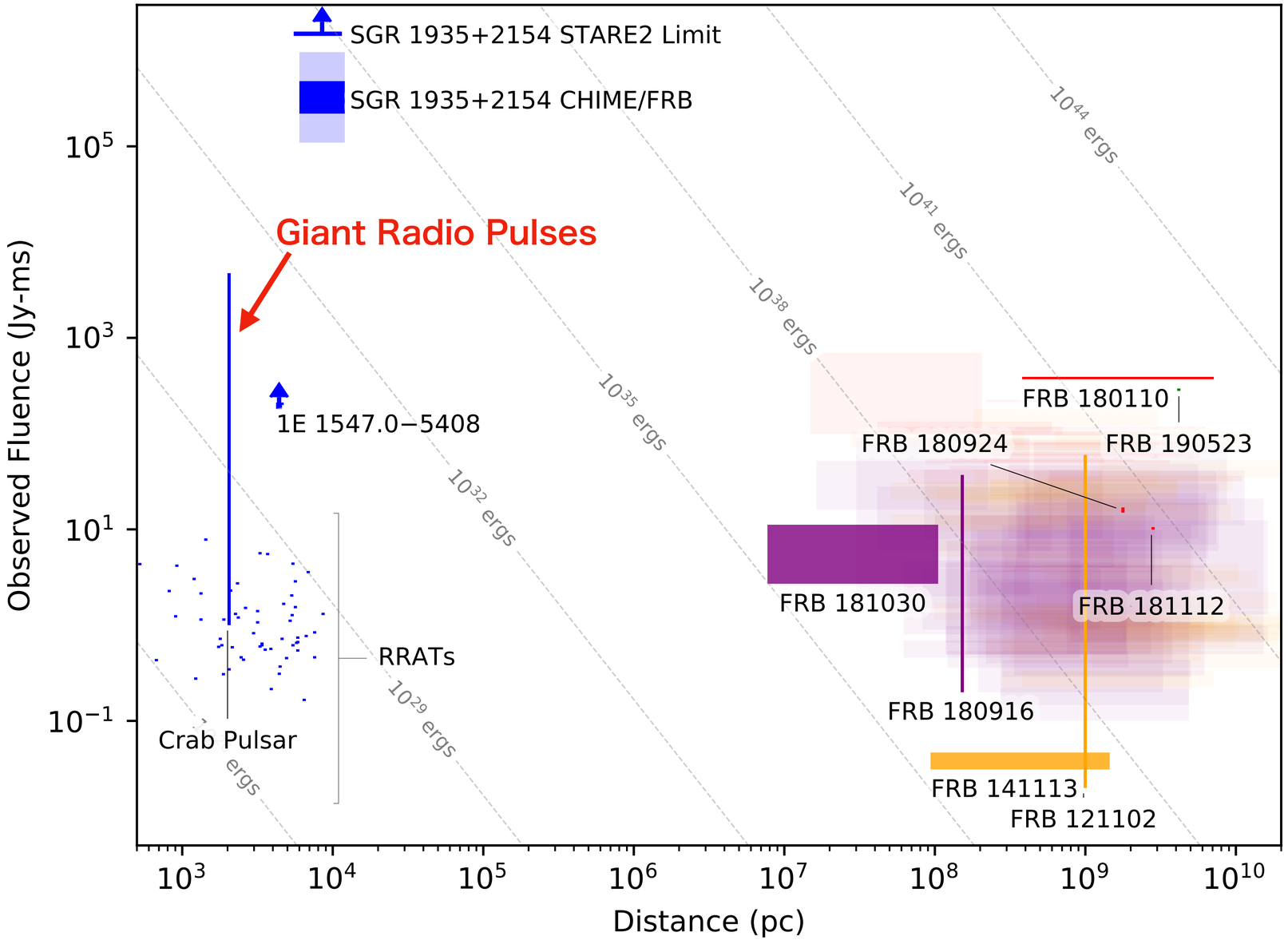

- Compared with extra-Galactic FRBs, this Galactic FRB is
  - Higher fluence
  - Lower luminosity
- Implication: FRB coherent (?) radio emission and incoherent X-ray burst are related with each other.

The CHIME/FRB Collaboration, arXiv:2005.10324

Giant radio Pulses (GPs) from rotation-powered pulsars

- Sporadic sub-millisecond radio bursts $10^{2\text{-}3}$ times brighter than the normal pulses.
- Only from known ~12 sources, power-law distribution of fluence.
- Fast radio bursts (FRBs) are extragalactic GPs from young and energetic pulsars?

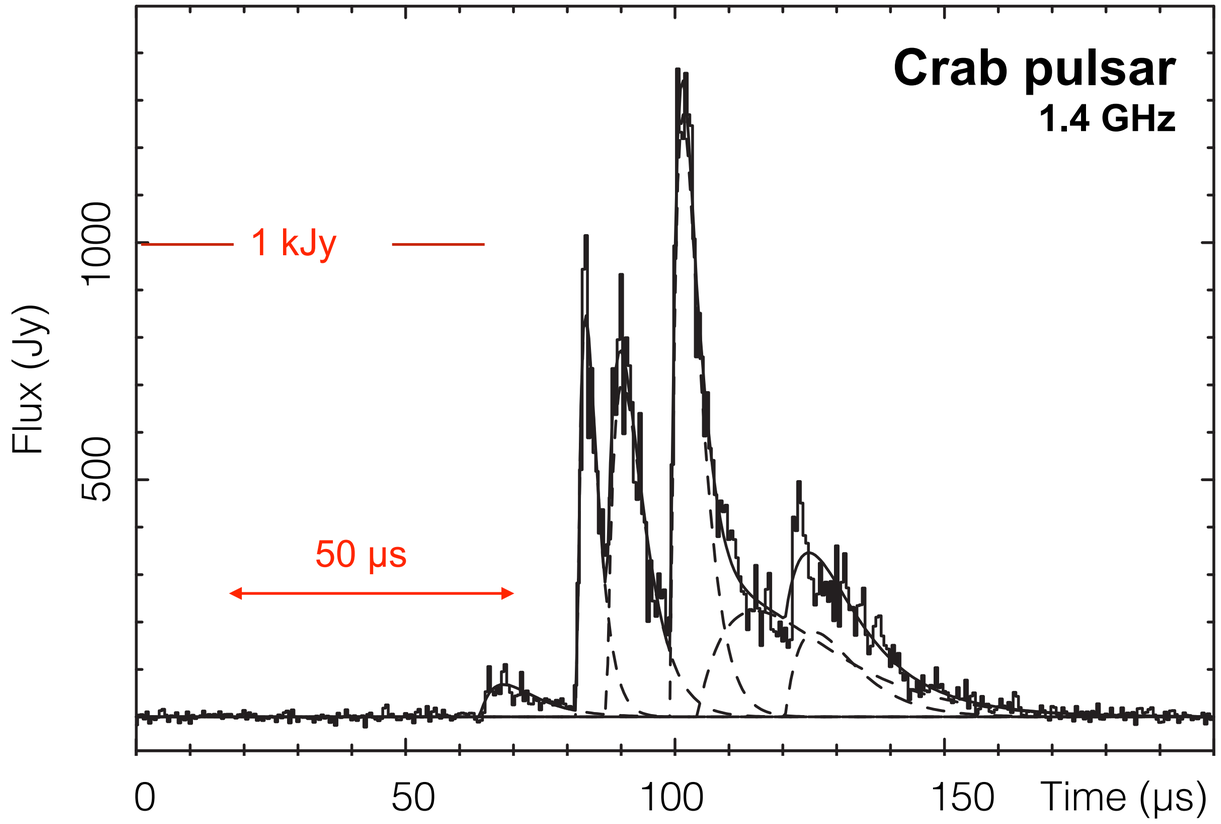

(Sallmen et al., 1999)

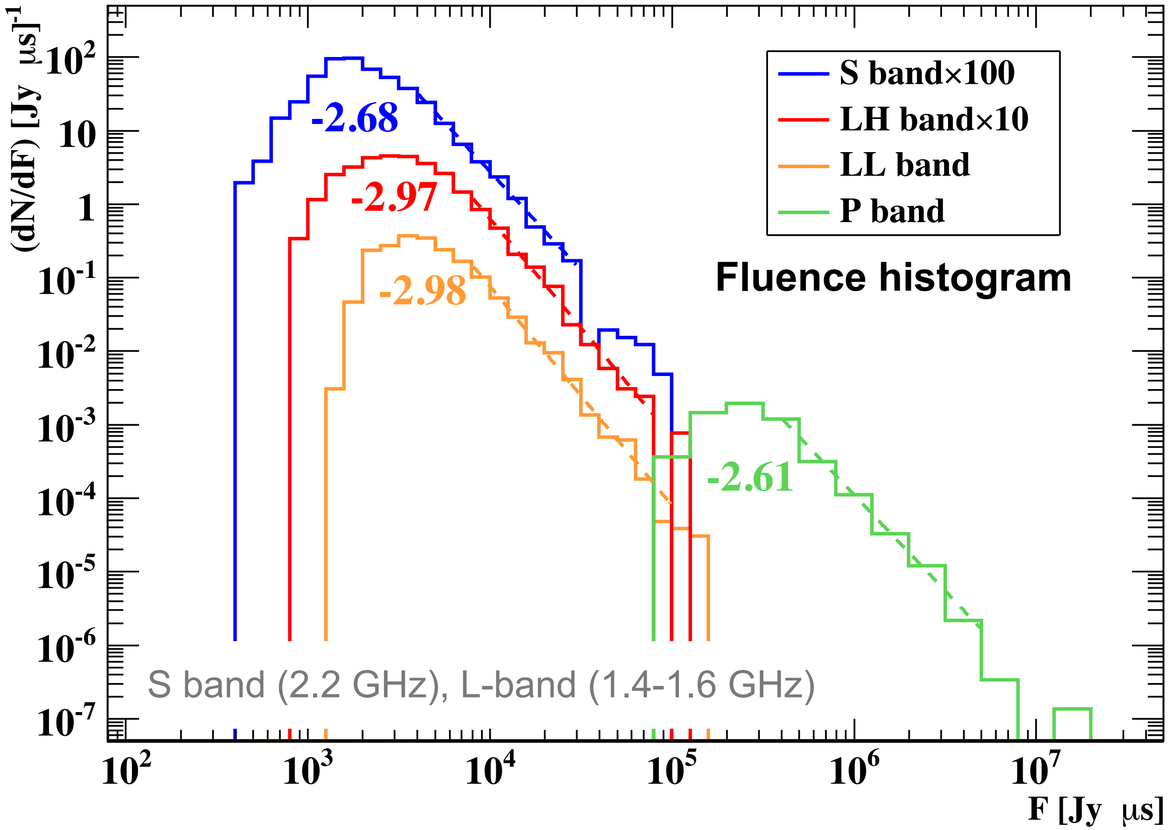

(Mikami et al., 2016)

GPs from the Crab Pulsar

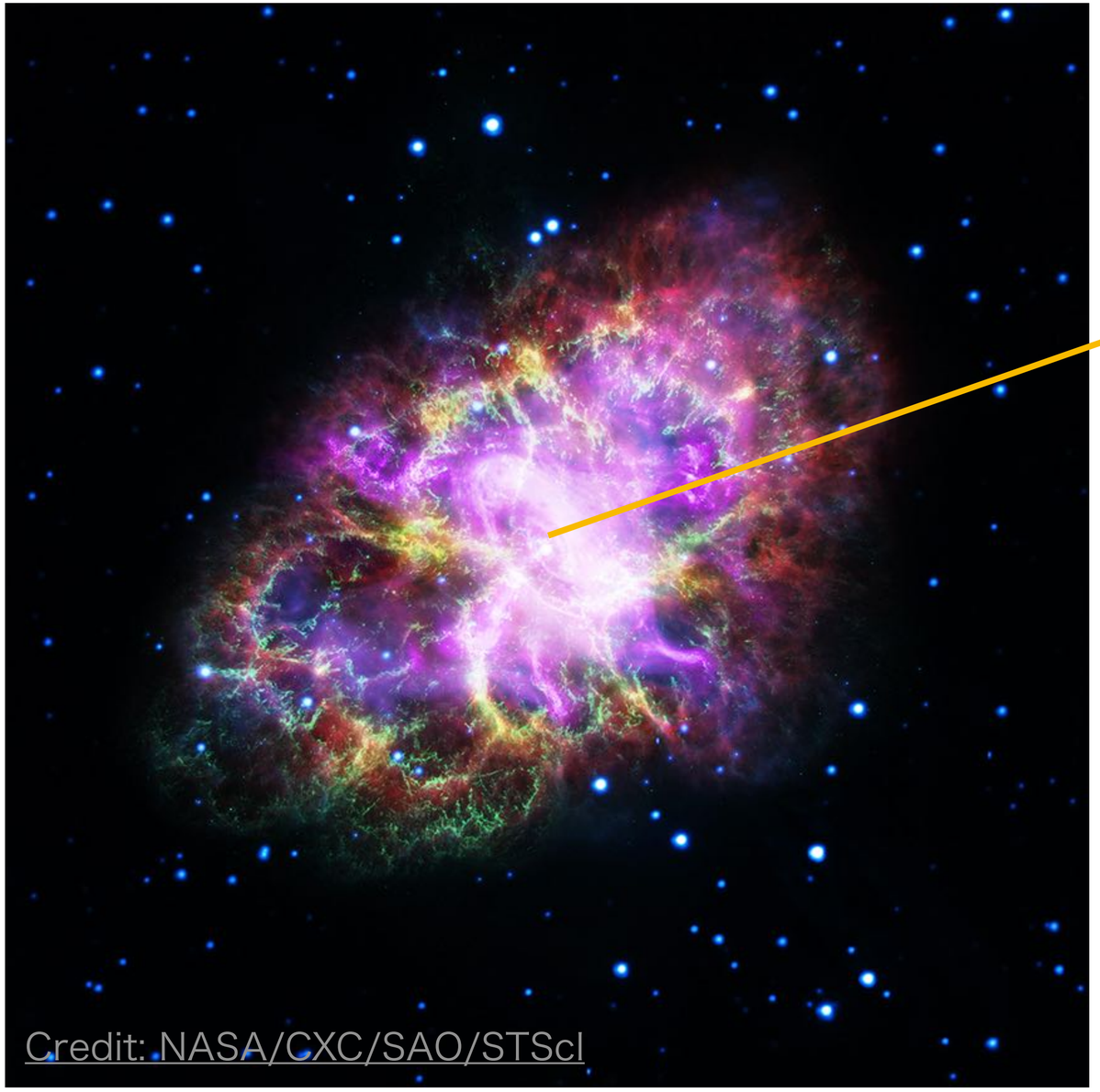

Credit: NASA/CXC/SAO/STScI

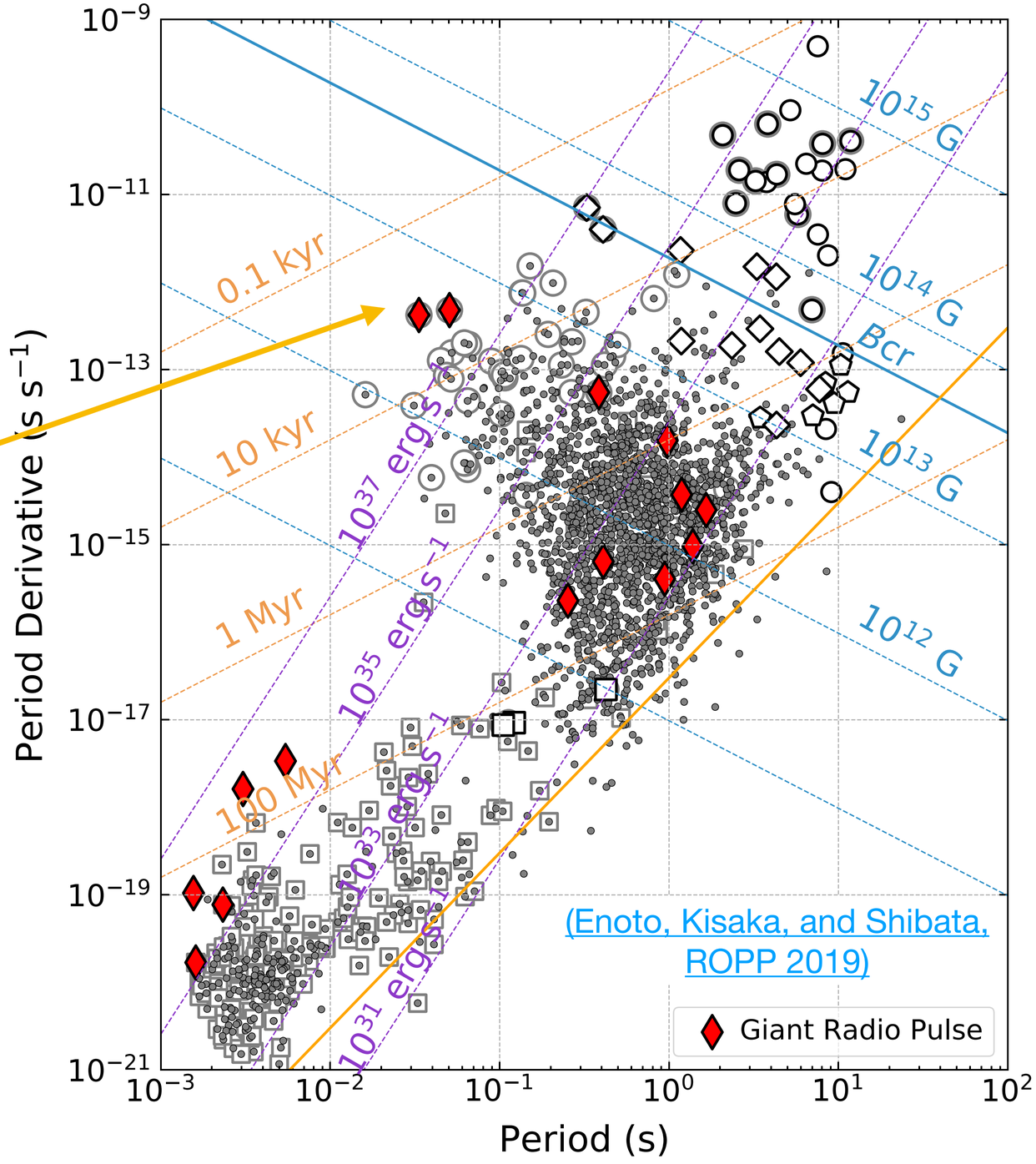

GPs from the Crab Pulsar

- Crab pulsar has been observed in almost all electromagnetic waves, including radio, infrared, optical, X-rays, and gamma rays.
- GPs of the Crab Pulsar randomly occur in the radio band at the main or inter pulses.
- GPs were thought to be a phenomenon observed only at radio. However optical enhancement coinciding with GPs was discovered (Shearer et al., Science 2003).
- Many teams have been trying to search for an enhancement in X-rays or gamma rays for 20 years, but only the upper limits have been obtained (Chandra, Suzaku…).

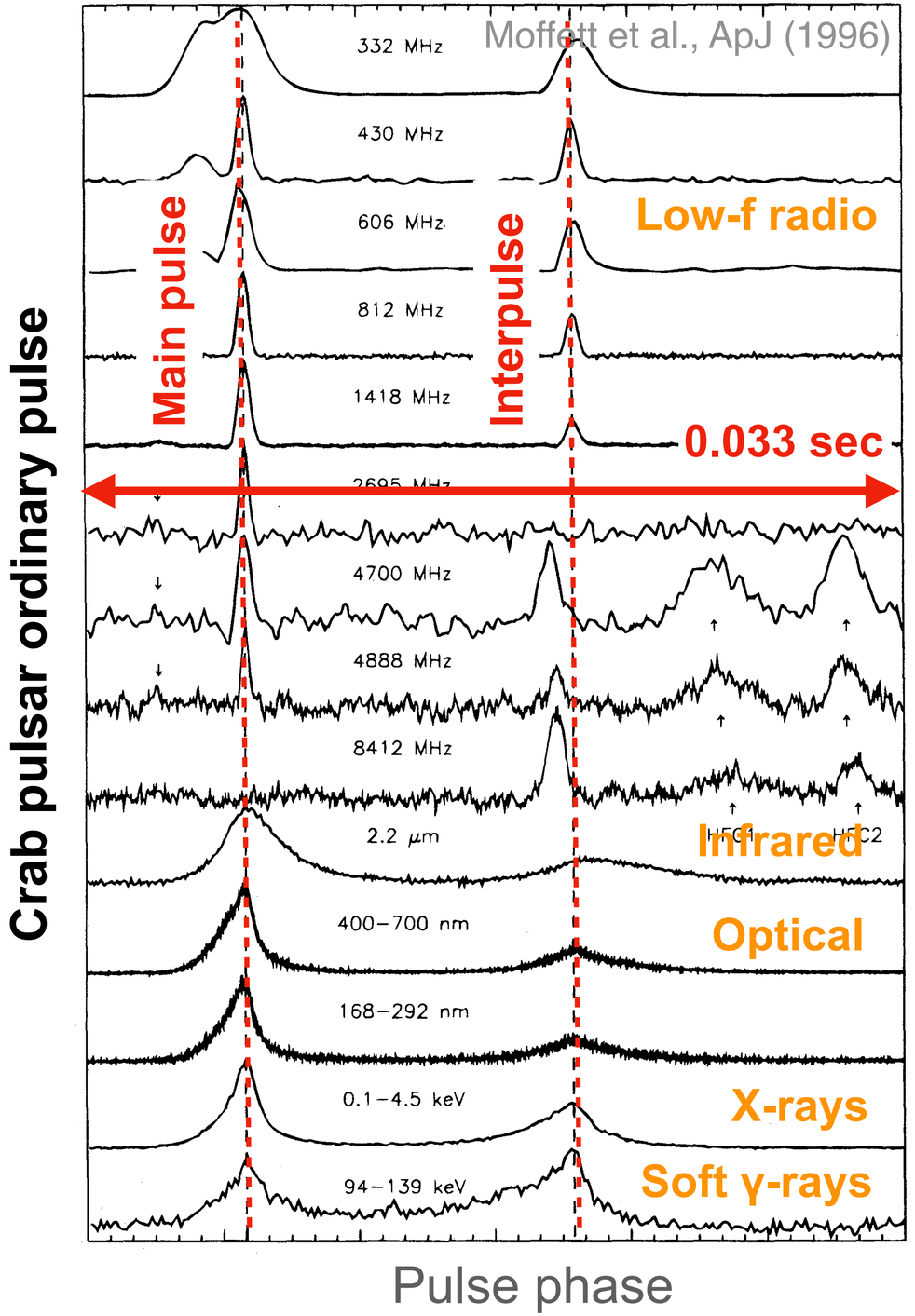

GPs from the Crab Pulsar

- Crab pulsar has been observed in almost all electromagnetic waves, including radio, infrared, optical, X-rays, and gamma rays.
- GPs of the Crab Pulsar randomly occur in the radio band at the main or inter pulses.
- GPs were thought to be a phenomenon observed only at radio. However optical enhancement coinciding with GPs was discovered (Shearer et al., Science 2003).
- Many teams have been trying to search for an enhancement in X-rays or gamma rays for 20 years, but only the upper limits have been obtained (Chandra, Suzaku…).

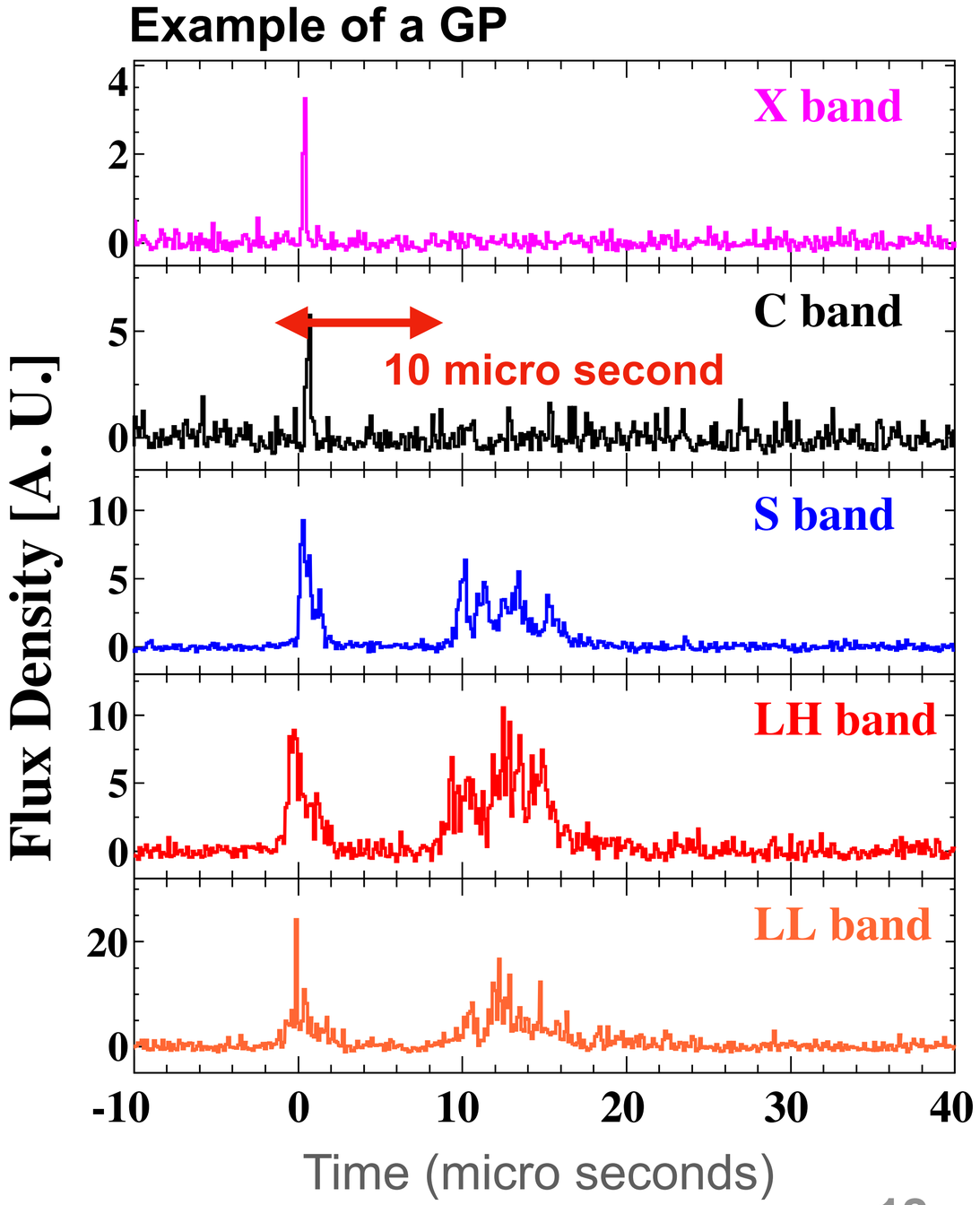

Mikami et al., ApJ (2016)

X-ray observatory NICER on the ISS

- The largest effective area 1,900 cm^2 at 1.5 keV with high-time resolution (<100 ns)!

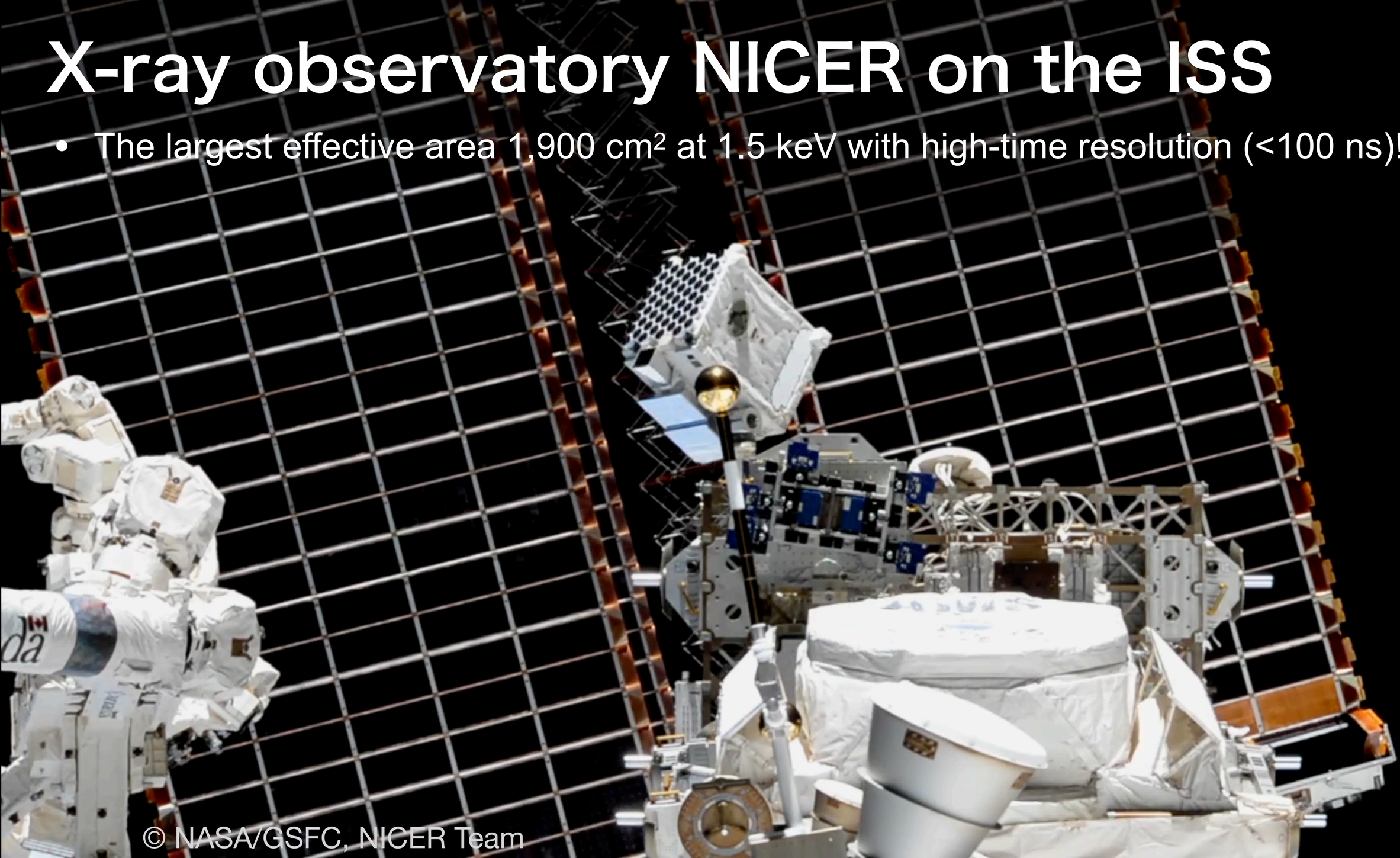

X-ray observatory NICER on the ISS

- The largest effective area 1,900 cm^2 at 1.5 keV with high-time resolution (<100 ns)!

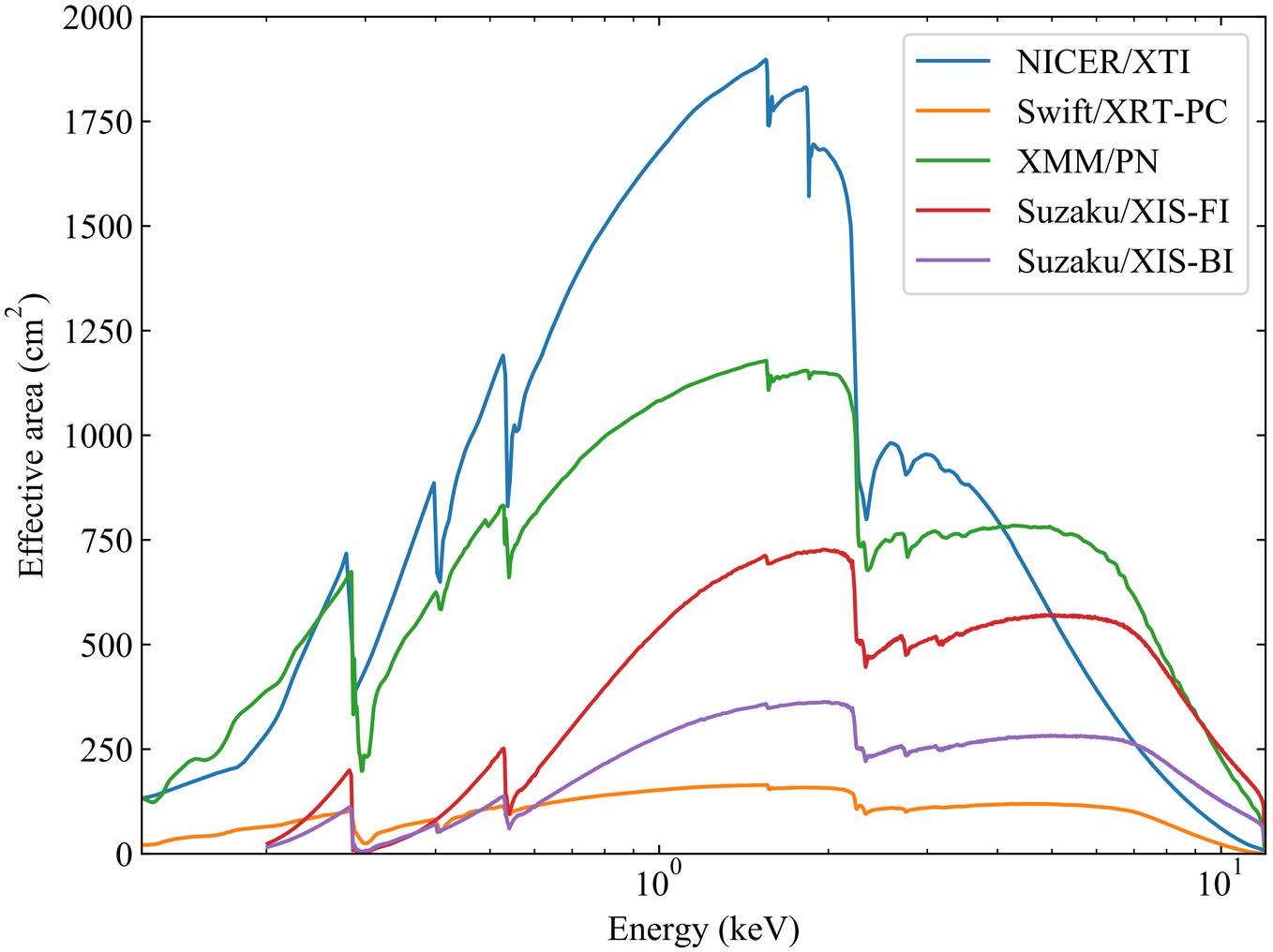

(K. Gendreau, et al., SPIE, 2012; Z. Arzoumanian, et al., SPIE, 2014)

Short exposure to detect the Crab pulsation

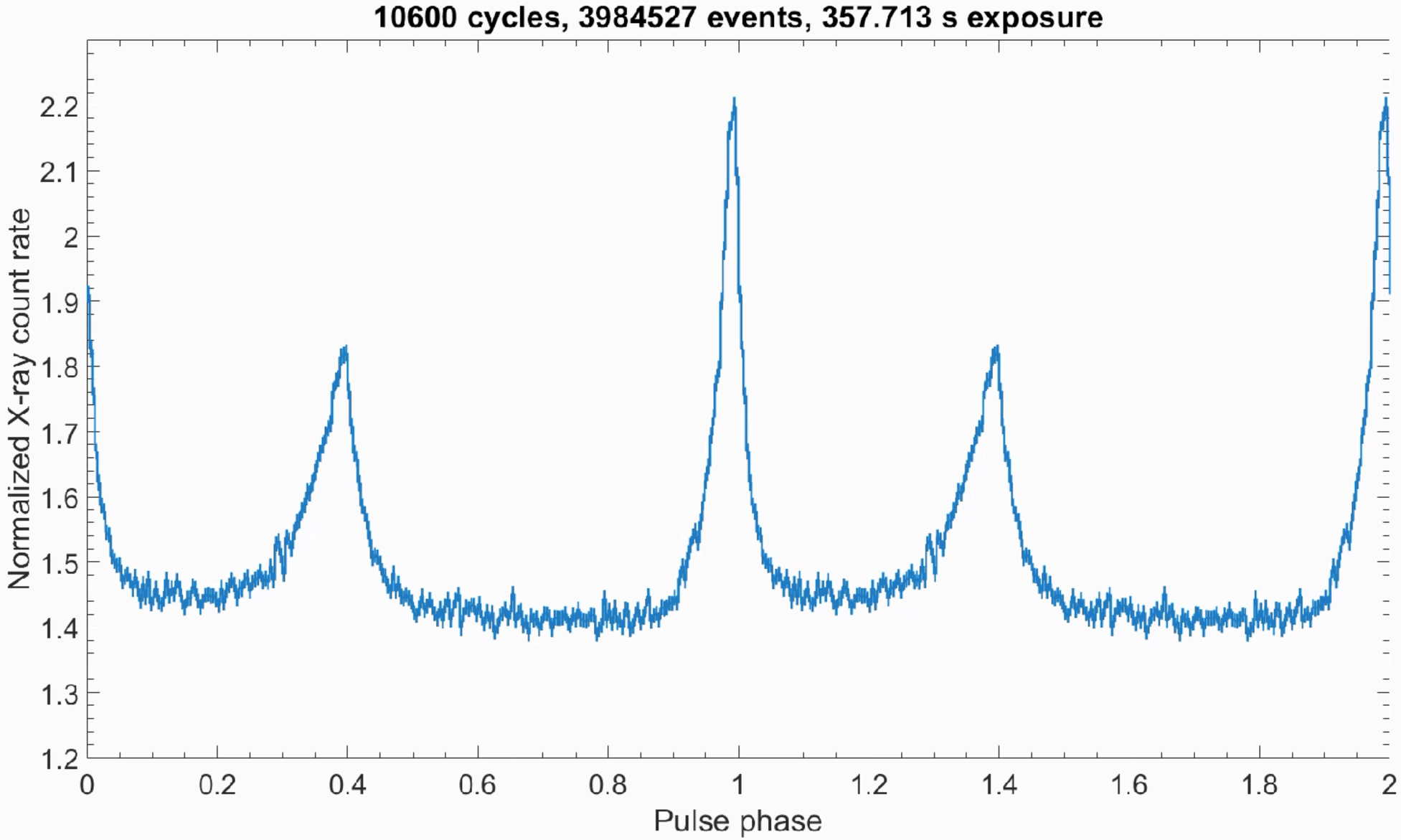

Short exposure to detect the Crab pulsation

Detection significance of X-ray pulses

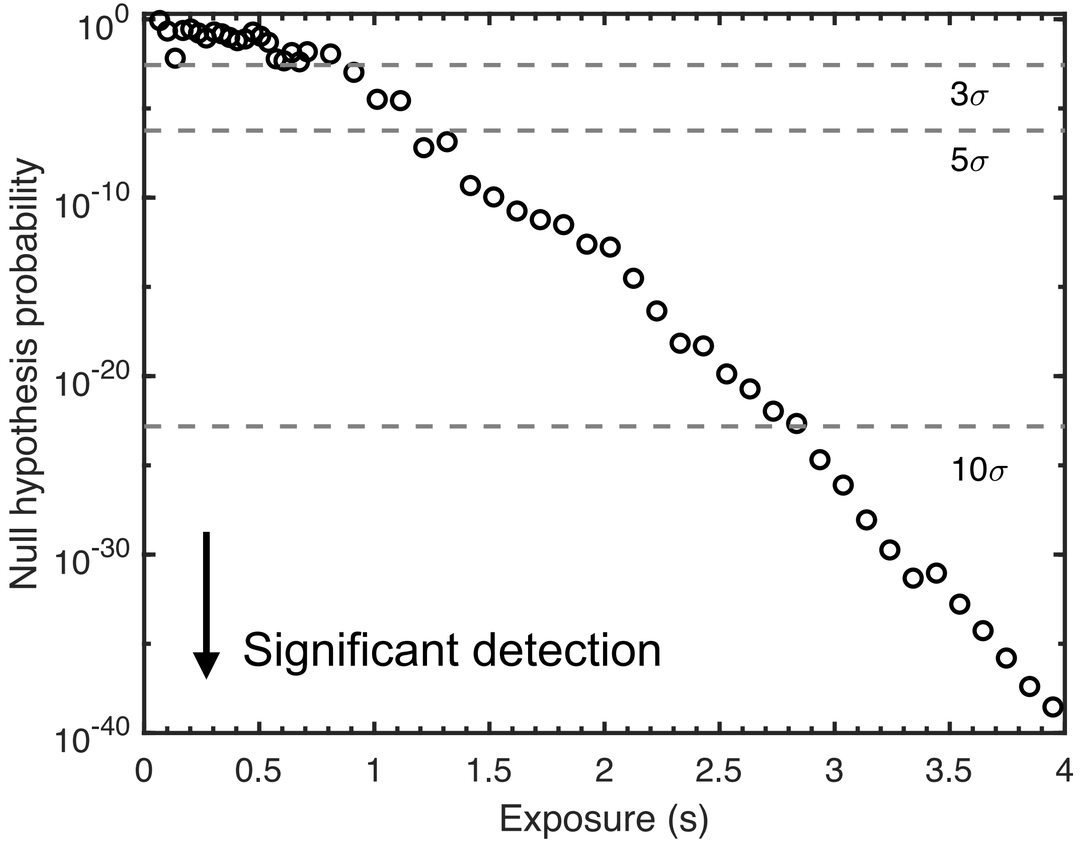

NICER X-ray spectrum of the Crab pulsar and nebula

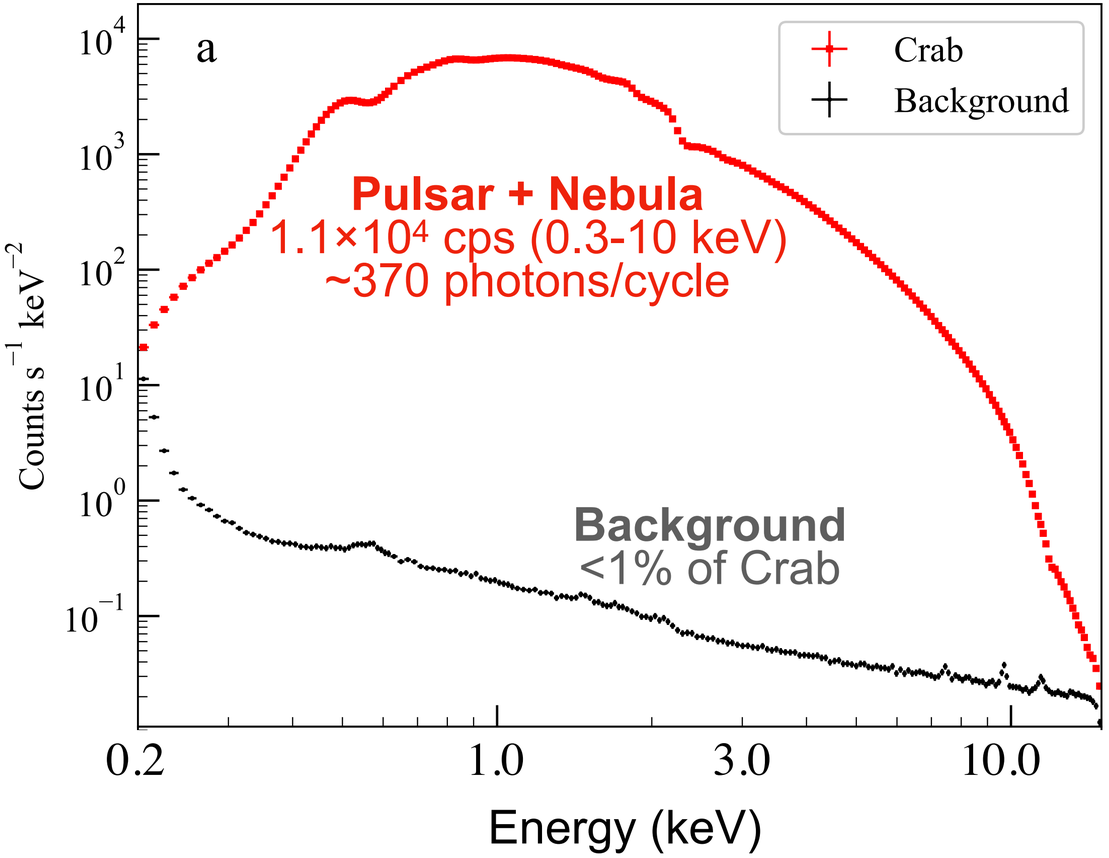

- Pulse signals are detectable within 1 sec, ×50 larger photon statistics than Hitomi.
- Free from pileups, dead time, and data transfer loss (throughput 3.8×10⁴ cps).

GPs from the Crab Pulsar

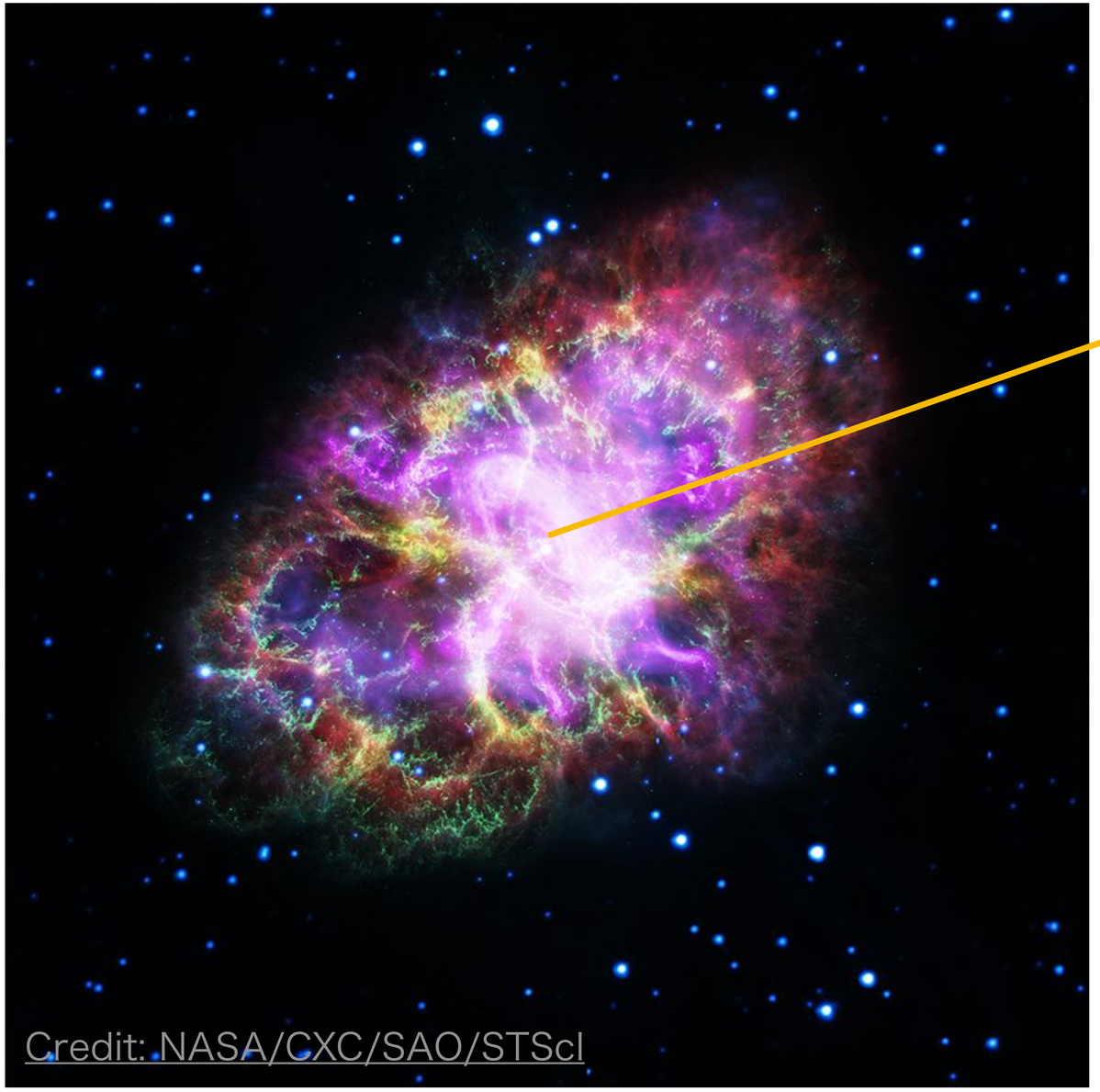

Credit: NASA/CXC/SAO/STScI

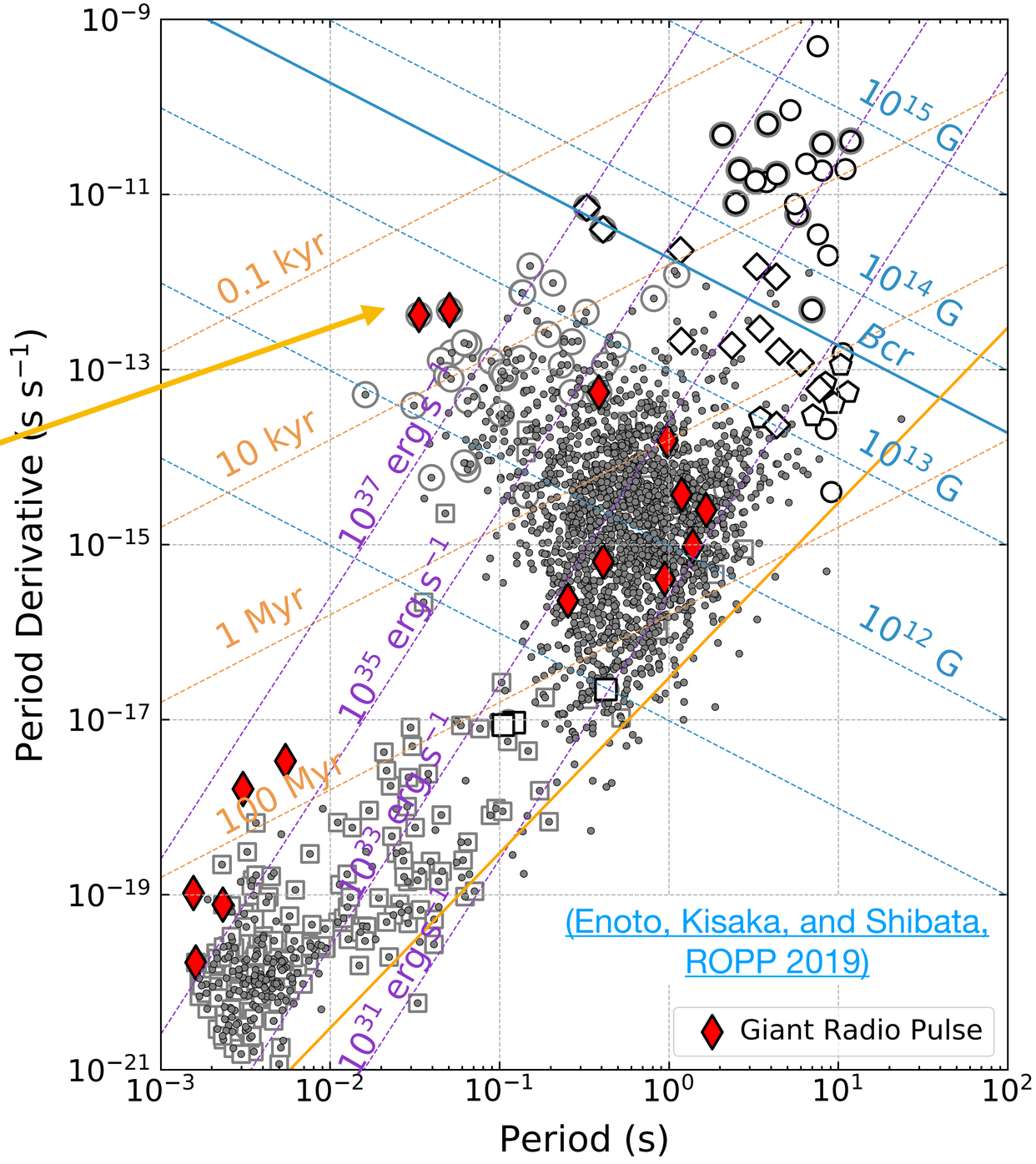

Two Radio Observatories (2 GHz) in Japan

(Credit) NICT/Kashima

- 34-m radio telescope of the Kashima Space Technology Center (NICT)


(Credit) JAXA/Usuda

- 64-m radio dish of the Usuda Deep Space Center (JAXA)

Long-term monitoring simultaneous in radio and X-rays

- Coordinated 15 observations with the two radio telescopes in 2017-2019
- The X-ray main pulse peak ϕ=0.9915±0.00004 relative to the radio peak, corresponding to the source-intrinsic 304 us radio delay.

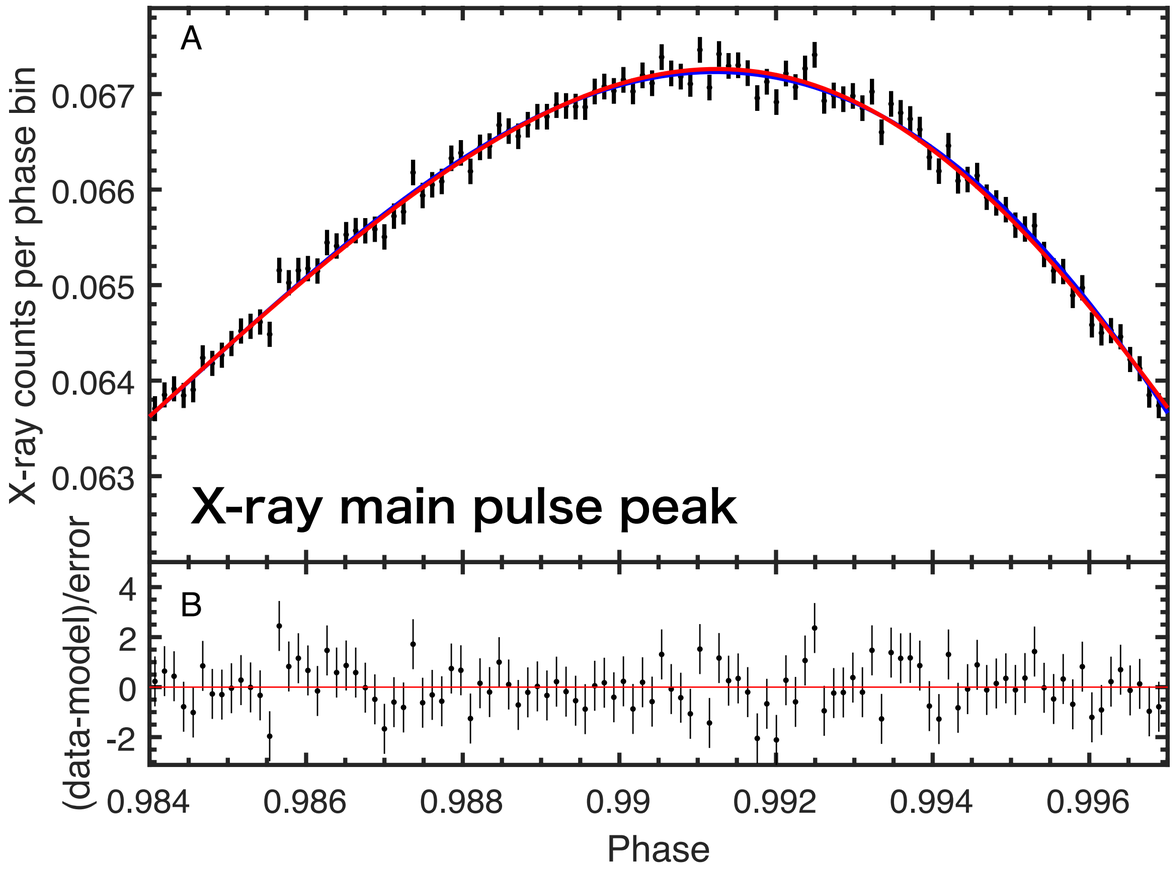

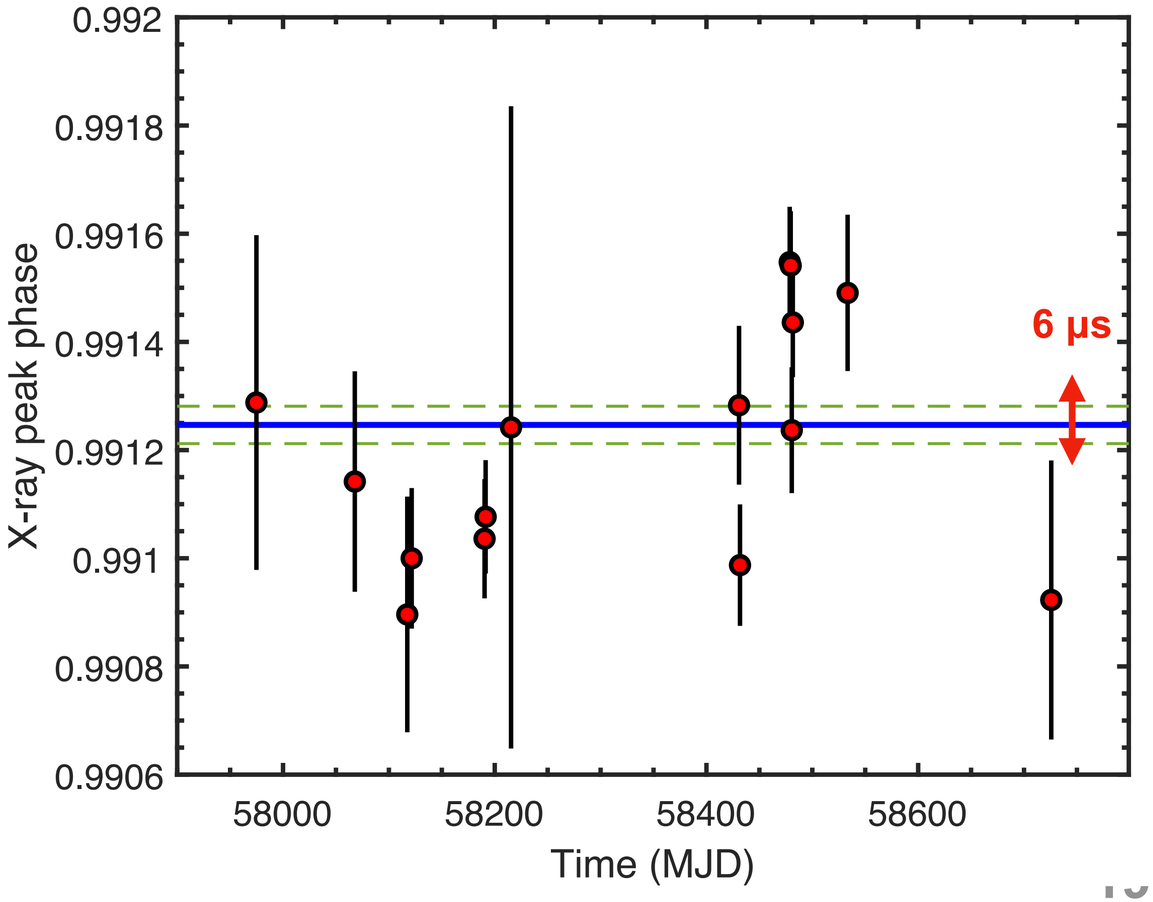

Discovery of X-ray enhancement coinciding with GPs

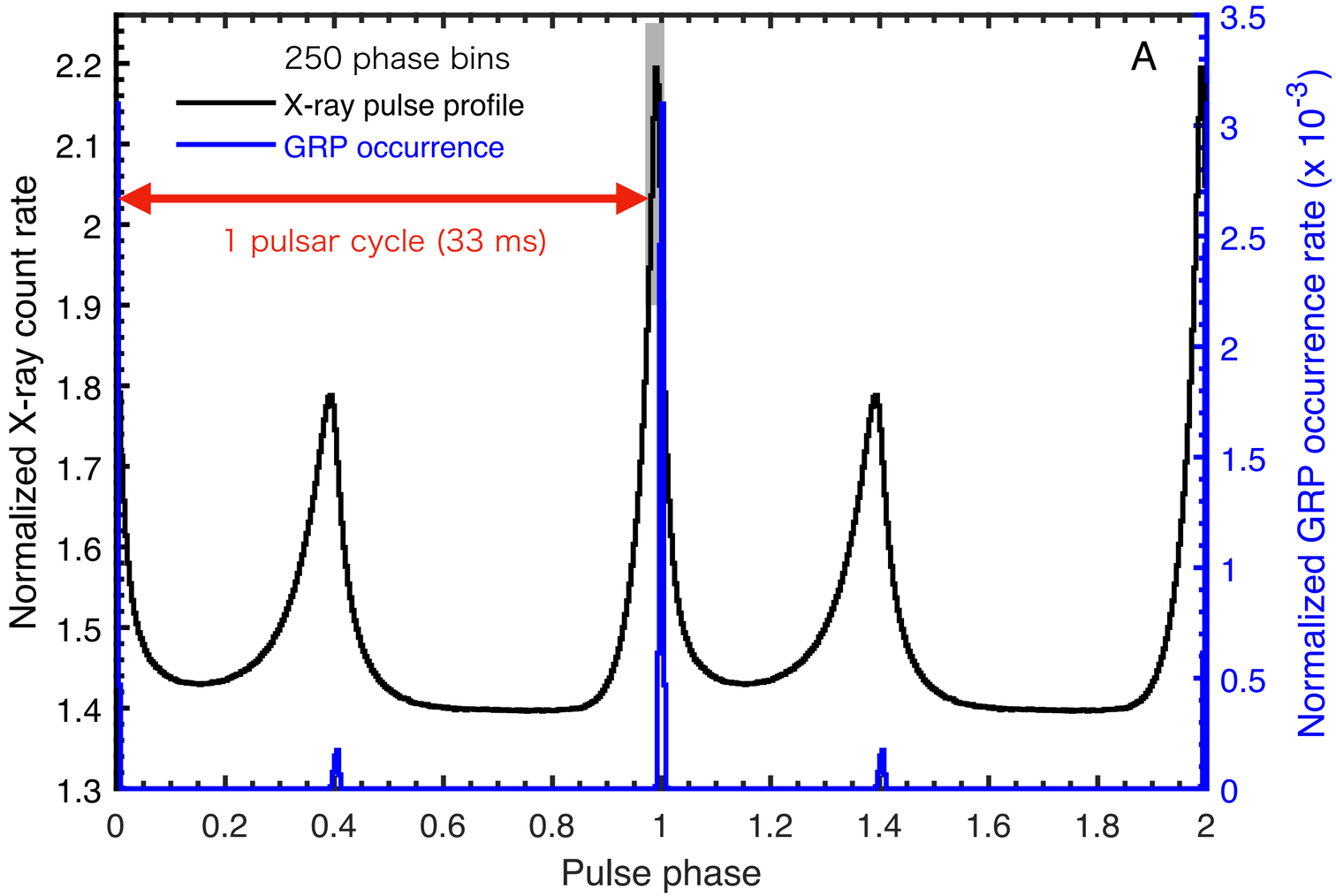

- Detected ~2.5×10^4 GPs at the main pulse phase with the 1.5-day exposure in total accumulated in 2017-2019.

Discovery of X-ray enhancement coinciding with GPs

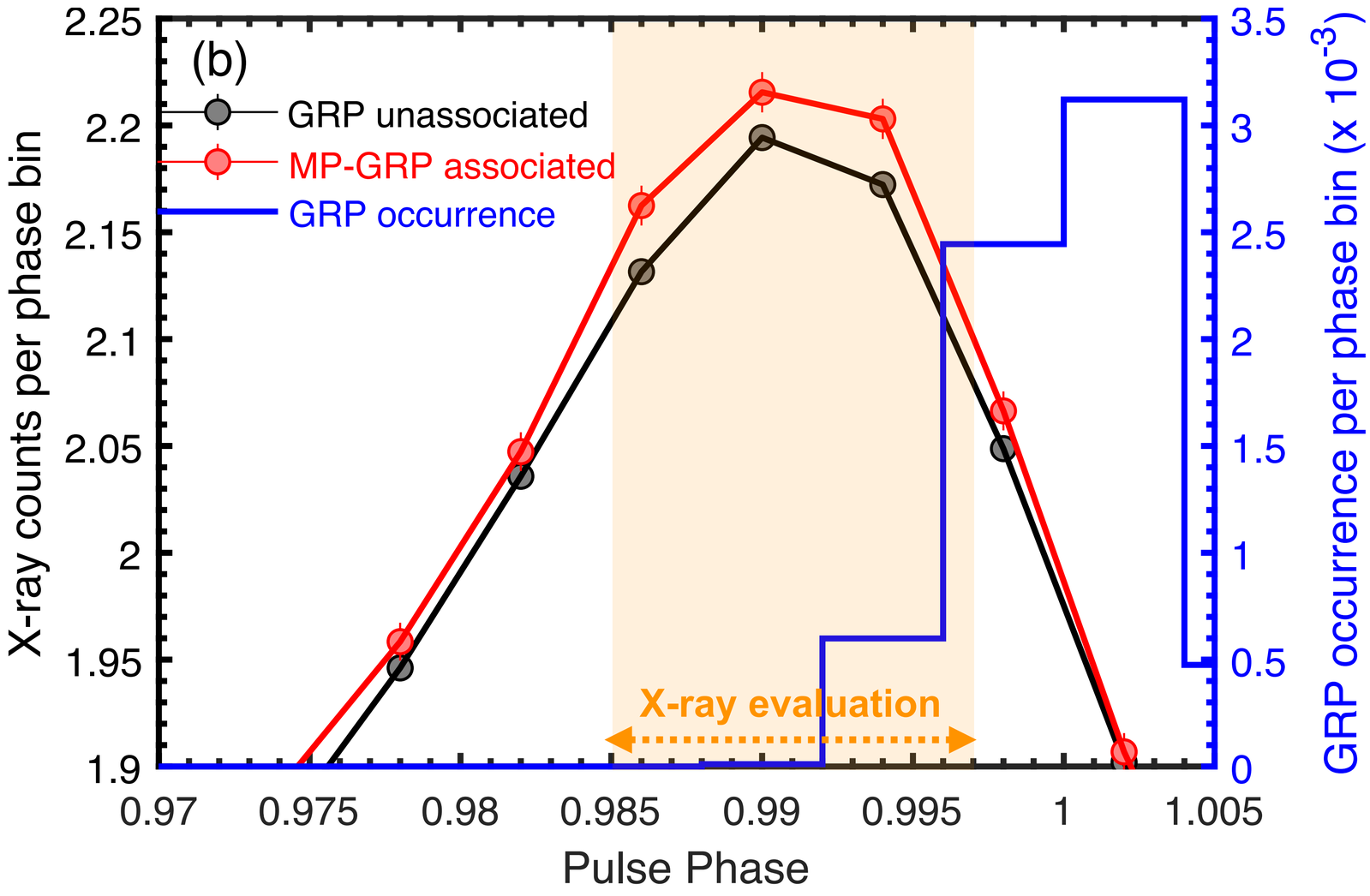

- X-ray enhancement of 3.8±0.7% (1σ error) at the pulse phase ϕ=0.985-0.997.

Discovery of X-ray enhancement coinciding with GPs

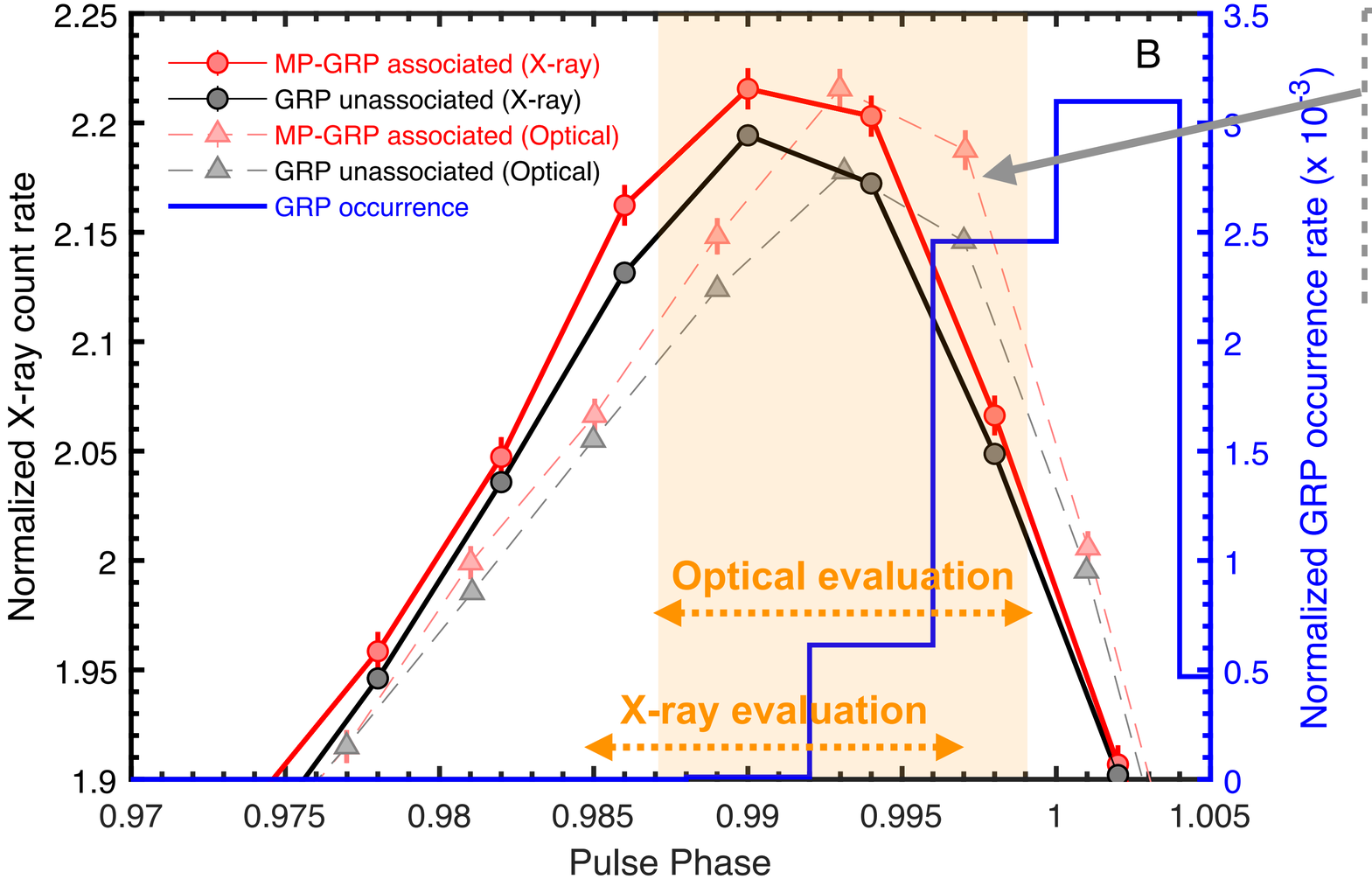

Optical enhancement
(Strader et al., ApJ 2013)

3.2±0.5%
(φ=0.987-0.999)

- X-ray enhancement of 3.8±0.7% (1σ error) at the pulse phase φ=0.985-0.997.

Verified our X-ray detection

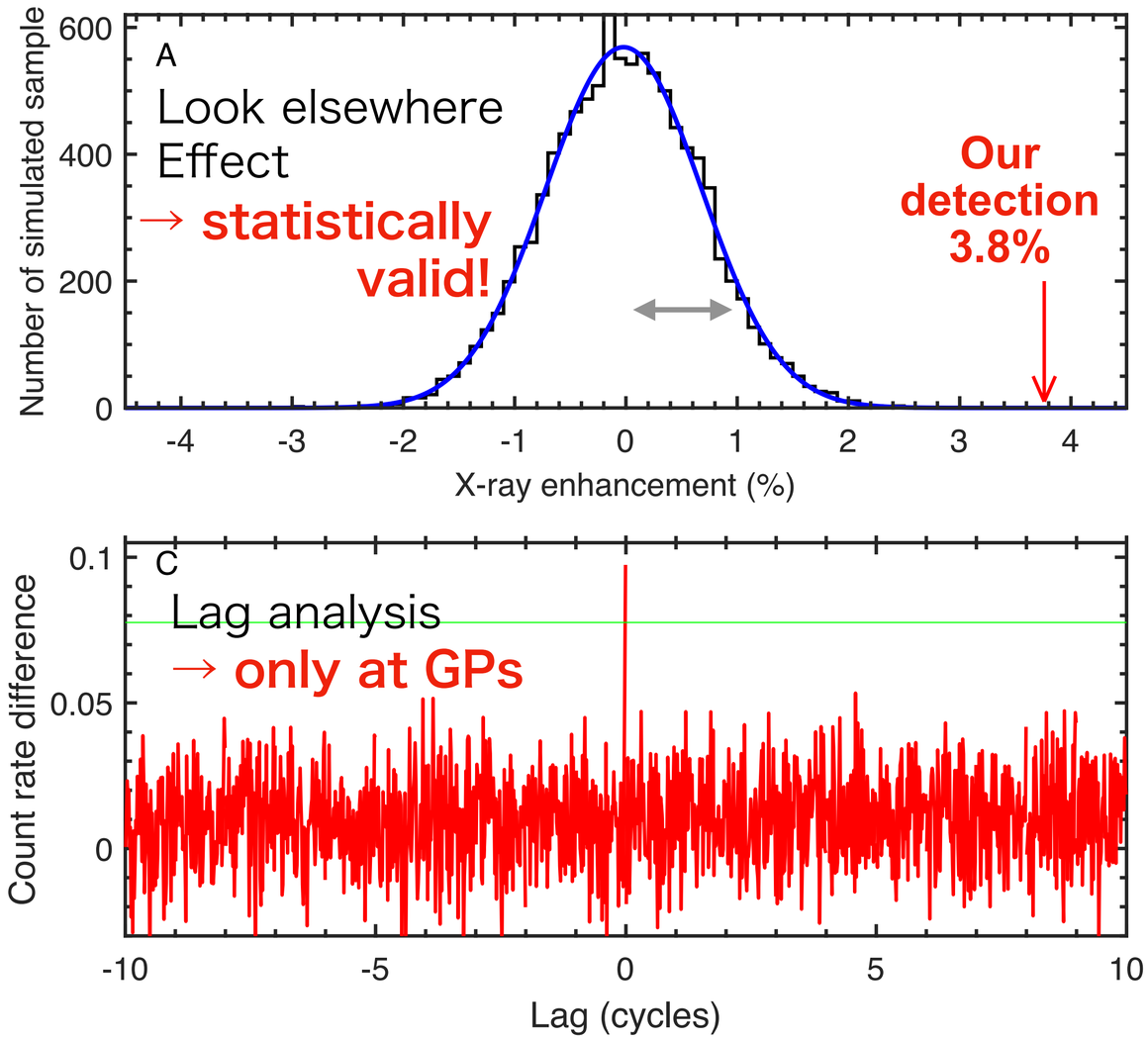

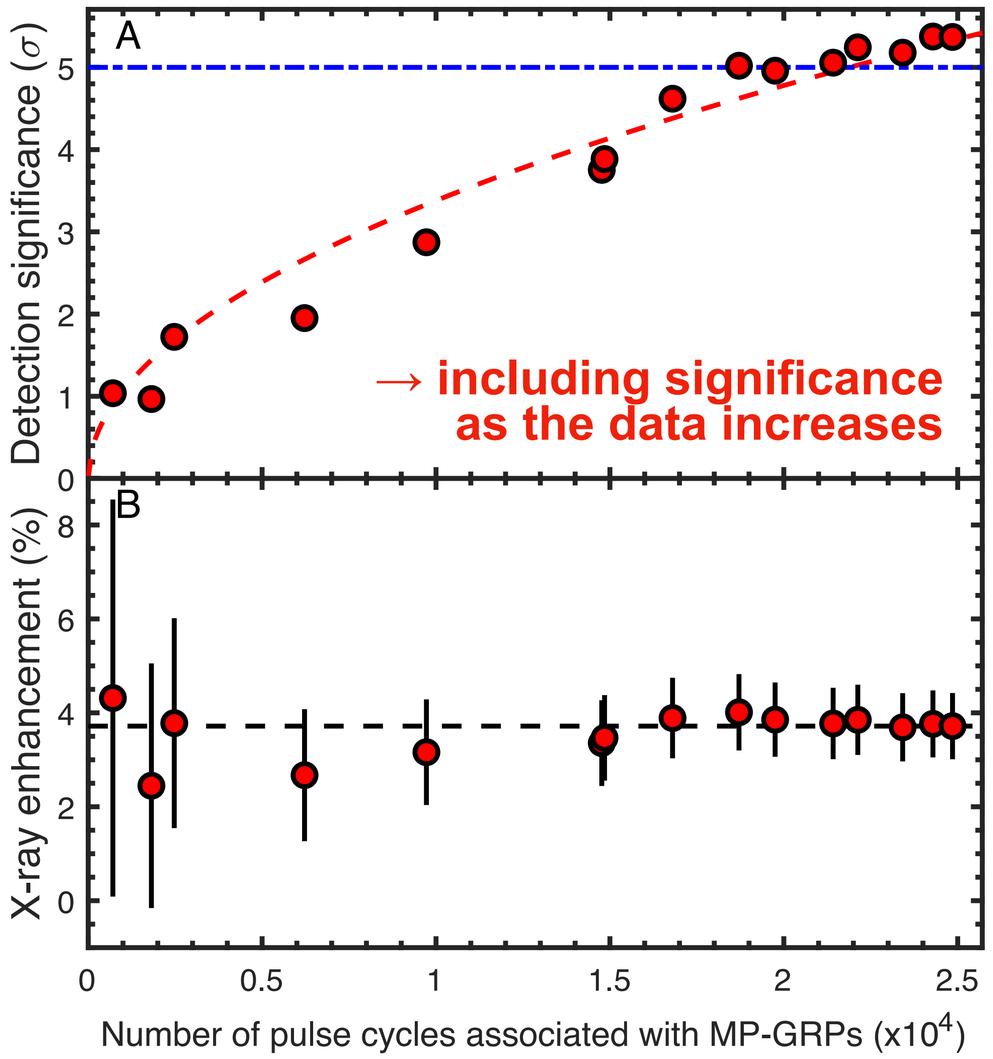

- We confirmed this detection via different verifications (see the paper).

Compared with previous observations

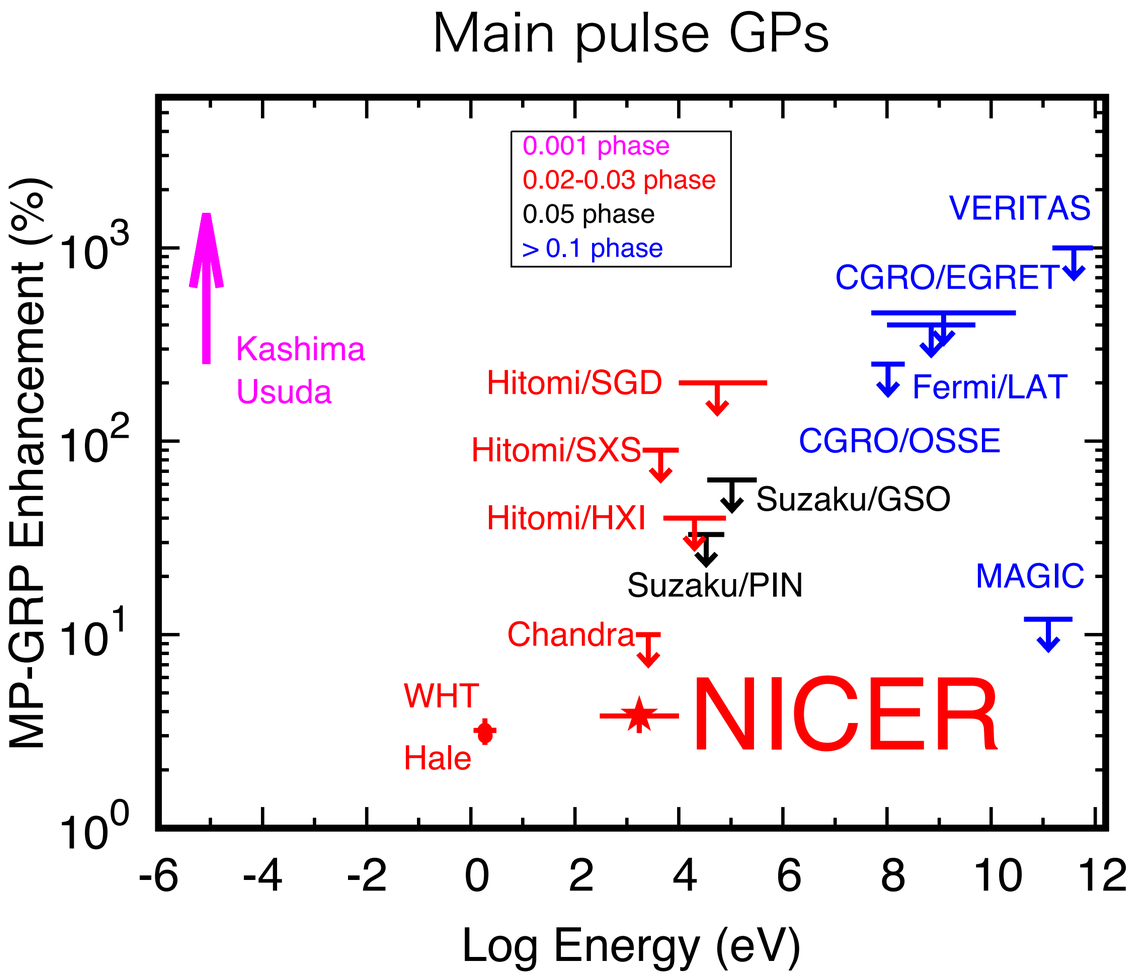

- Our X-ray detection is consistent with the previous upper limits in the X-rays (~10% or higher limits)
- X-ray enhancement (3.8%) is at the same as that in the optical detection (3.2%).
- Only the upper limit (<10%, 3σ) for the interpulse GPs at ϕ= 1.378-1.402.

Compared with previous observations

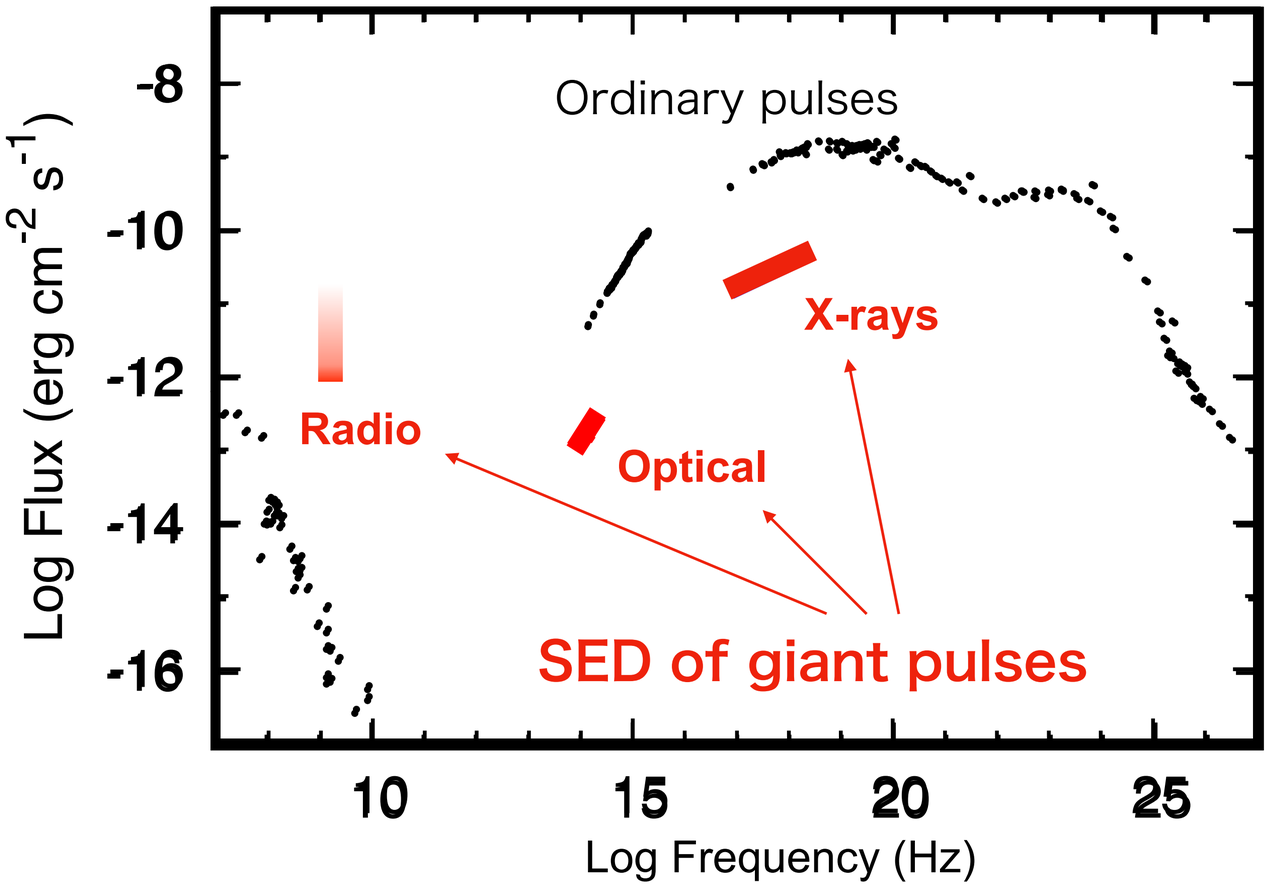

- High-energy pulsar component (optical and X-rays) is distinct from the radio coherent component.
- No difference of the GP-associated X-ray spectrum from the normal pulses.
- X-ray flux of the pulsar component 4.4×10^{-9} ergs/s/cm2 (0.3-10 keV) is 10^3 and 10^7 times higher than those at the optical (5,500A) and radio (2 GHz) bands, respectively.
- **Despite ~4% enhancement, the total emitted energy at GPs is 10-10^2 larger than we previously know.**

Emission mechanism of GPs?

- The emission mechanism of normal radio pulses and GPs is still a mystery.
- Amplification factor at GP is ~10^2-10^3 times at the radio band, while those for the optical and X-rays are an imbalance at only 4%!
- Since radio waves are coherent radiation, they require aligned motions, states and a dense plasma.

Coherent radiation
(radio)

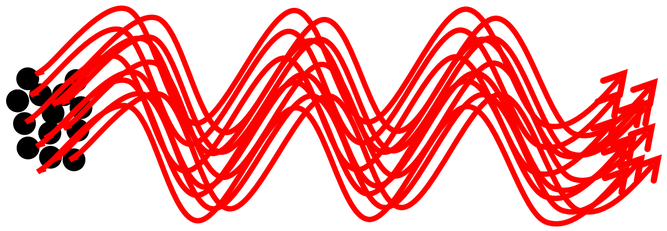

Since the phase is nearly aligned,
the intensity is proportional to
the **square** of the number of particles.

Incoherent radiation
(Optical and X-rays)

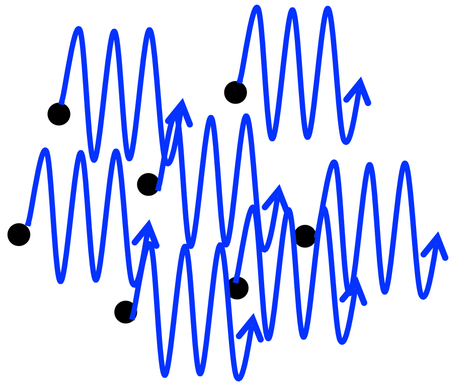

Since the phase is not aligned,
the intensity is proportional to
the number of particles.

Emission mechanism of GPs? (One Hypothesis)

- A sheet of dense plasma is formed in the outer part of the pulsar magnetosphere.
- The plasma sheet is structurally unstable and tear apart to form plasma blobs.
- The blobs repeatedly collide and merge, and sometimes grow to ~100 times (thickness).
- As the blobs coalesce, radio pulses are generated in the dense region, while X-rays are emitted from the entire sheet.

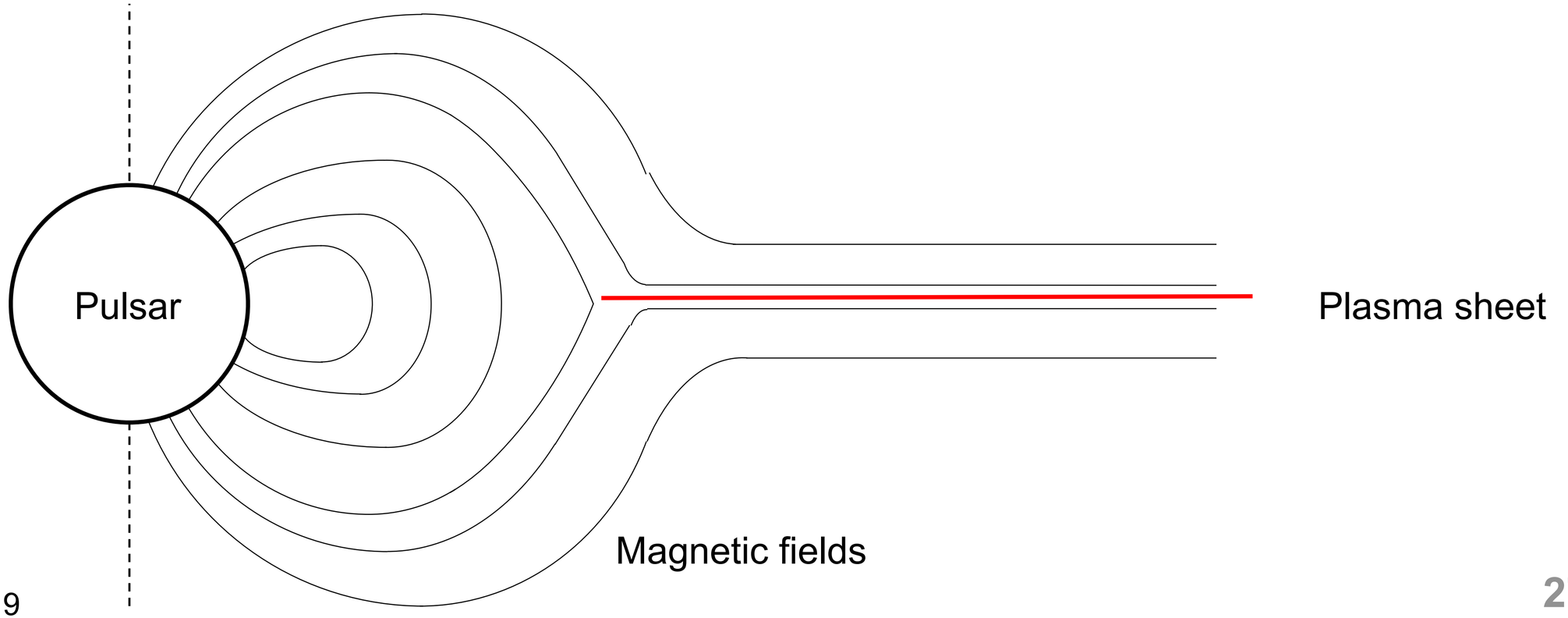

Based on
Philippov et al. ApJL 2019

Emission mechanism of GPs? (One Hypothesis)

- A sheet of dense plasma is formed in the outer part of the pulsar magnetosphere.
- The plasma sheet is structurally unstable and tear apart to form plasma blobs.
- The blobs repeatedly collide and merge, and sometimes grow to ~100 times (thickness).
- As the blobs coalesce, radio pulses are generated in the dense region, while X-rays are emitted from the entire sheet.

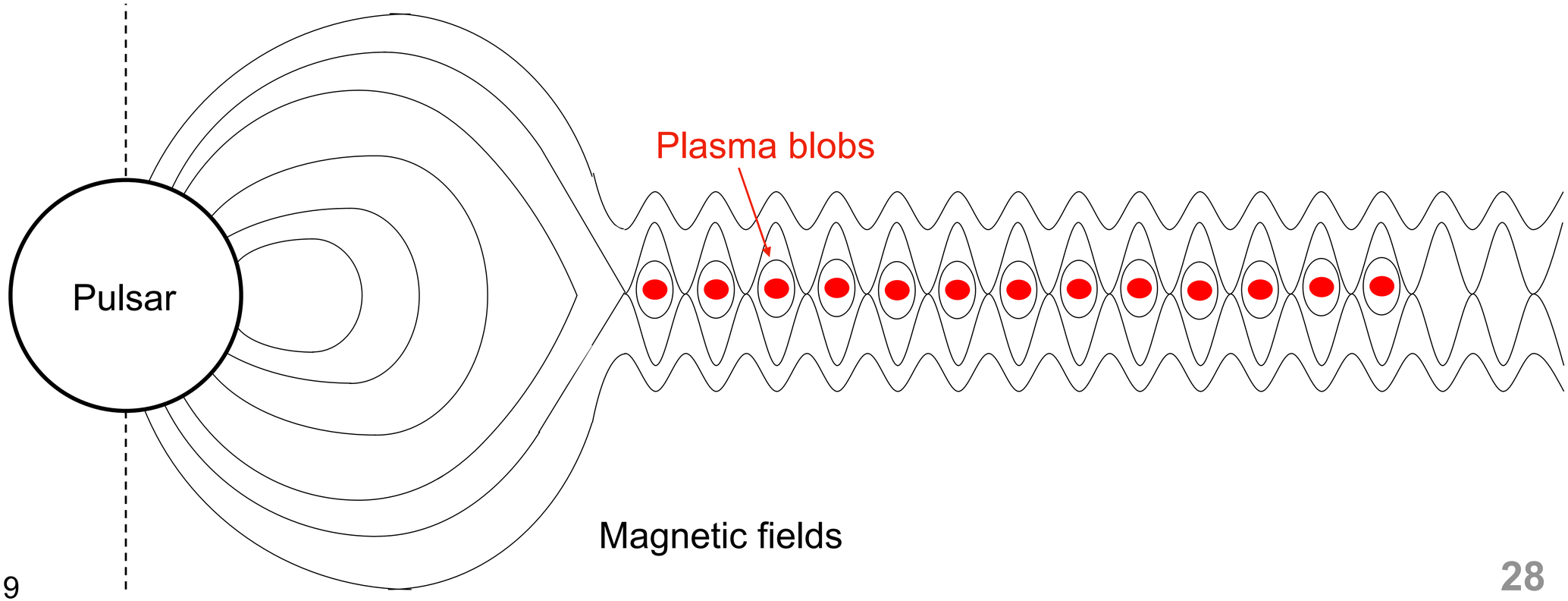

Based on
Philippov et al. ApJL 2019

Emission mechanism of GPs? (One Hypothesis)

- Numerical simulation of plasma blobs (from Sironi & Spitkovsky 2014 ApJL 783 L21)

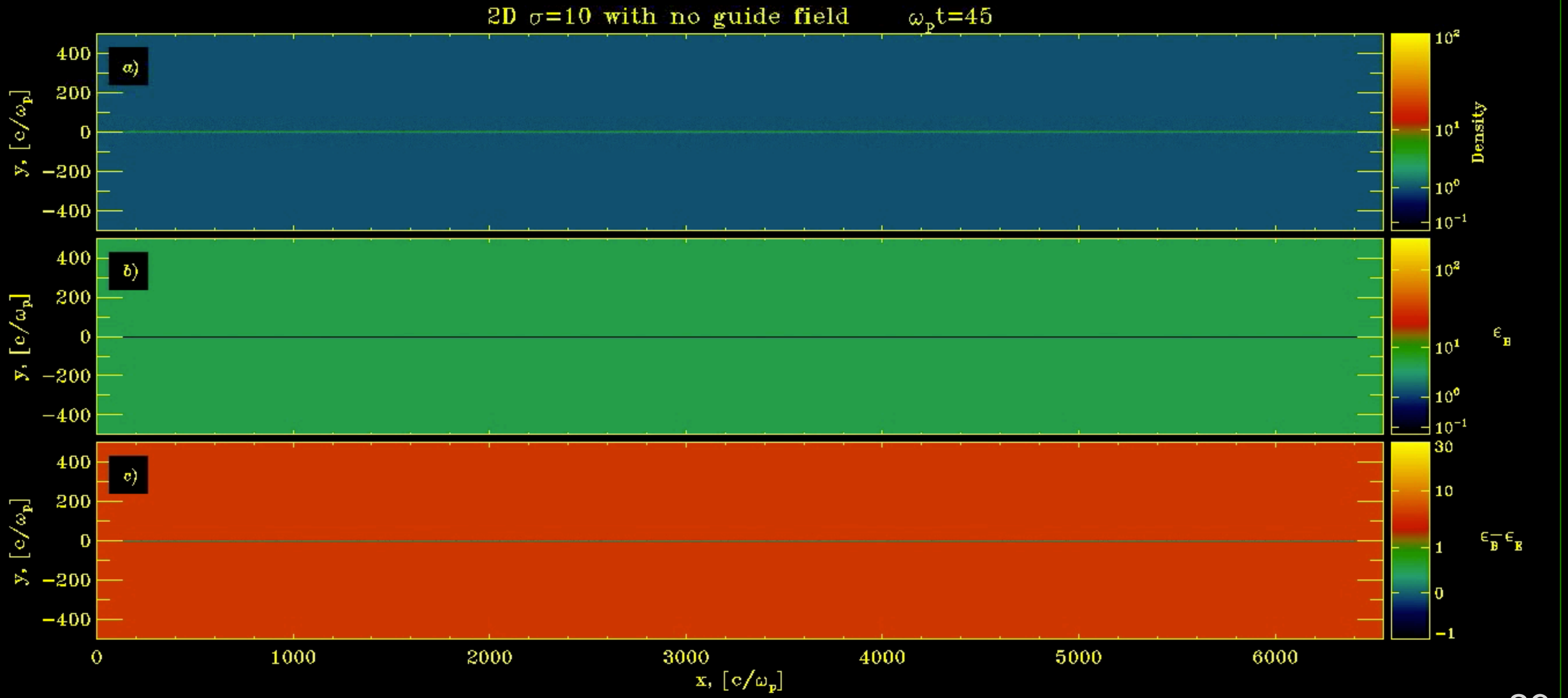

Emission mechanism of GPs? (One Hypothesis)

- A sheet of dense plasma is formed in the outer part of the pulsar magnetosphere.
- The plasma sheet is structurally unstable and tear apart to form plasma blobs.
- The blobs repeatedly collide and merge, and sometimes grow to ~100 times (thickness).
- As the blobs coalesce, radio pulses are generated in the dense region, while X-rays are emitted from the entire sheet.

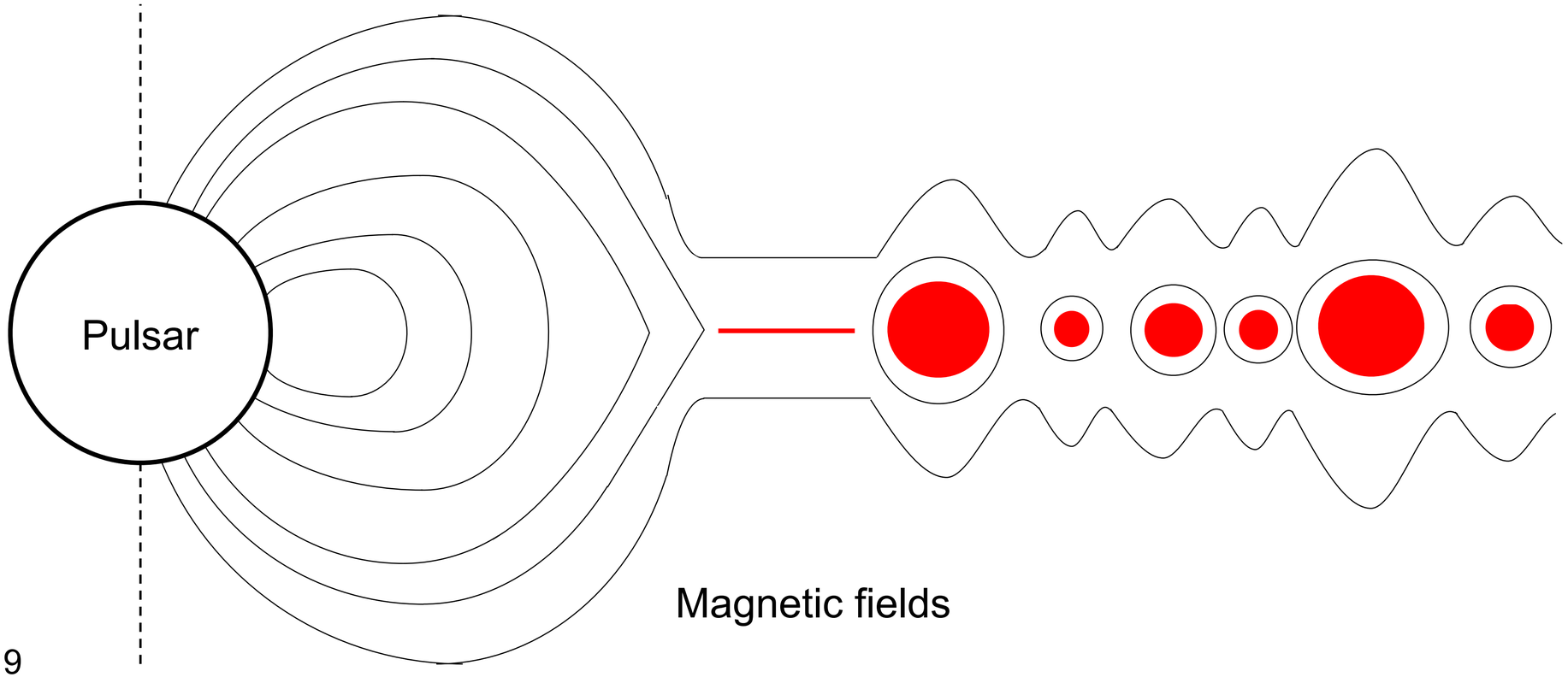

Based on
Philippov et al. ApJL 2019

Emission mechanism of GPs? (One Hypothesis)

- A sheet of dense plasma is formed in the outer part of the pulsar magnetosphere.
- The plasma sheet is structurally unstable and tear apart to form plasma blobs.
- The blobs repeatedly collide and merge, and sometimes grow to ~100 times (thickness).
- As the blobs coalesce, radio pulses are generated in the dense region, while X-rays are emitted from the entire sheet.

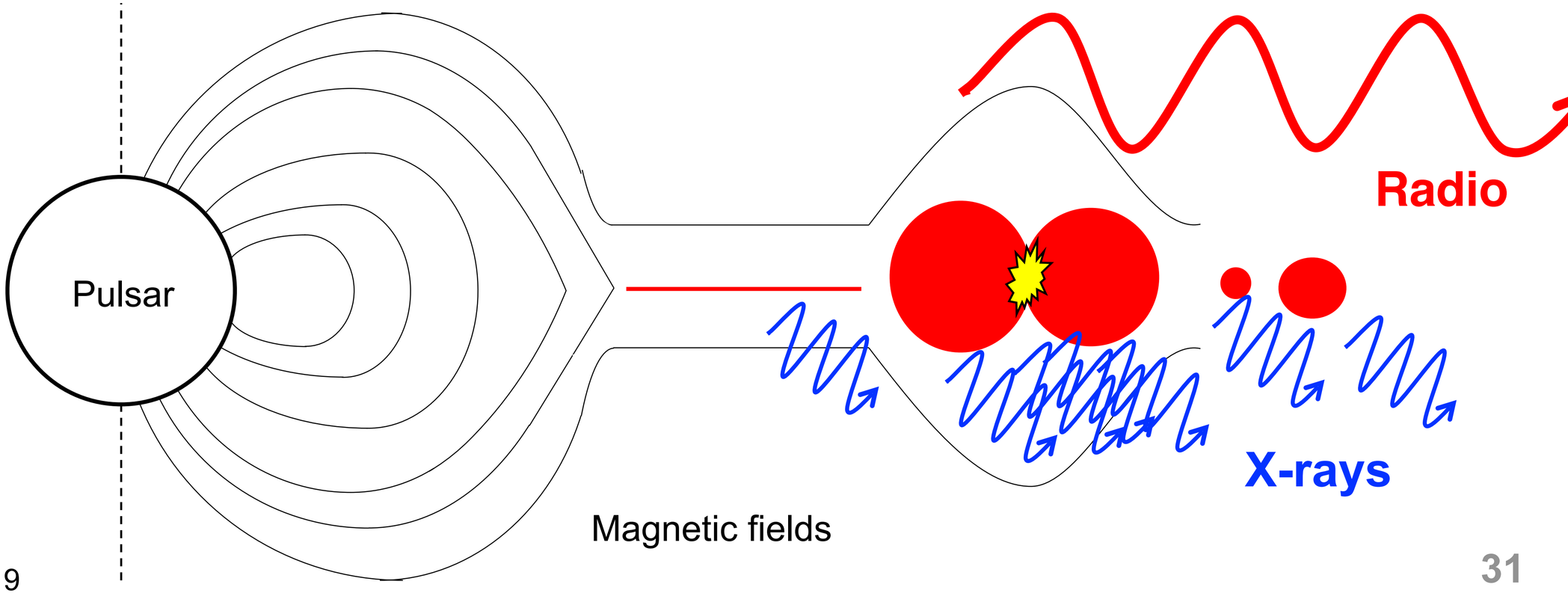

Based on
Philippov et al. ApJL 2019

Implication for the mystery of FRBs

- Hypothetical bright GRP is a candidate for the origin of FRBs, especially repeating FRB sources (e.g., repeating FRB 121102).
- The energy source of such FRBs is assumed to be the spin-down luminosity.
- The discovery of X-ray enhancement suggests:
  - Since bolometric luminosity of GPs, including X-rays, is revealed to be $10^{2\text{-}3}$ times higher than we previously thought, the simple GRP model for FRBs became more difficult because pulsars quickly lose its rotational energy.
  - Another example of the connection between the coherent radio emission and incoherent X-ray radiation in the neutron star magnetosphere. This is also shown the FRB-associated bursts from SGR 1935+2154. Burst activities of magnetars (magnetic energy release) is more favored for FRBs?

See the supplementary part of Enoto et al., Science 2021
Kashiyama & Murase, 2017; Kisaka, Enoto, Shibata 2017

… End of the Kashima Radio Observatory Operation

- The Kashima 34-m radio telescope, operated by the National Institute of Information and Communications Technology (NICT), has been an important instrument for radio astronomy.
- It was severely damaged by Typhoon No. 15 in 2019 and its operation was terminated.
- This achievement is one of the last precious legacies left by the Kashima 34 m radio telescope.
- We are looking forward to have another chance to collaborate with other radio telescopes as well.

Panel removal (September 2019)

Summary

1. The electromagnetic radiation mechanism from pulsars still has many unsolved problems. Giant pulses (GPs) are sporadic radio bursts 100-1000 times brighter than the normal radio pulses, and thus a powerful probe to investigate a pulsar magnetosphere within a single rotation.

2. NICER Magnetar and Magnetosphere (M&M) working group coordinated a simultaneous X-ray and radio observation campaign for the Crab pulsar in 2017-2019. We detected the X-ray enhancement by 3.8±0.7% (5.4σ detection) coinciding with radio GPs at the main pulse phase.

3. This implies that the total emitted energy from GPs is tens to hundreds of times higher than previously known. Repeating fast radio bursts are difficult to be explained by a model based on hypothesized bright GPs powered by the rotational energy loss. Young magnetars are favored?

Thank you!

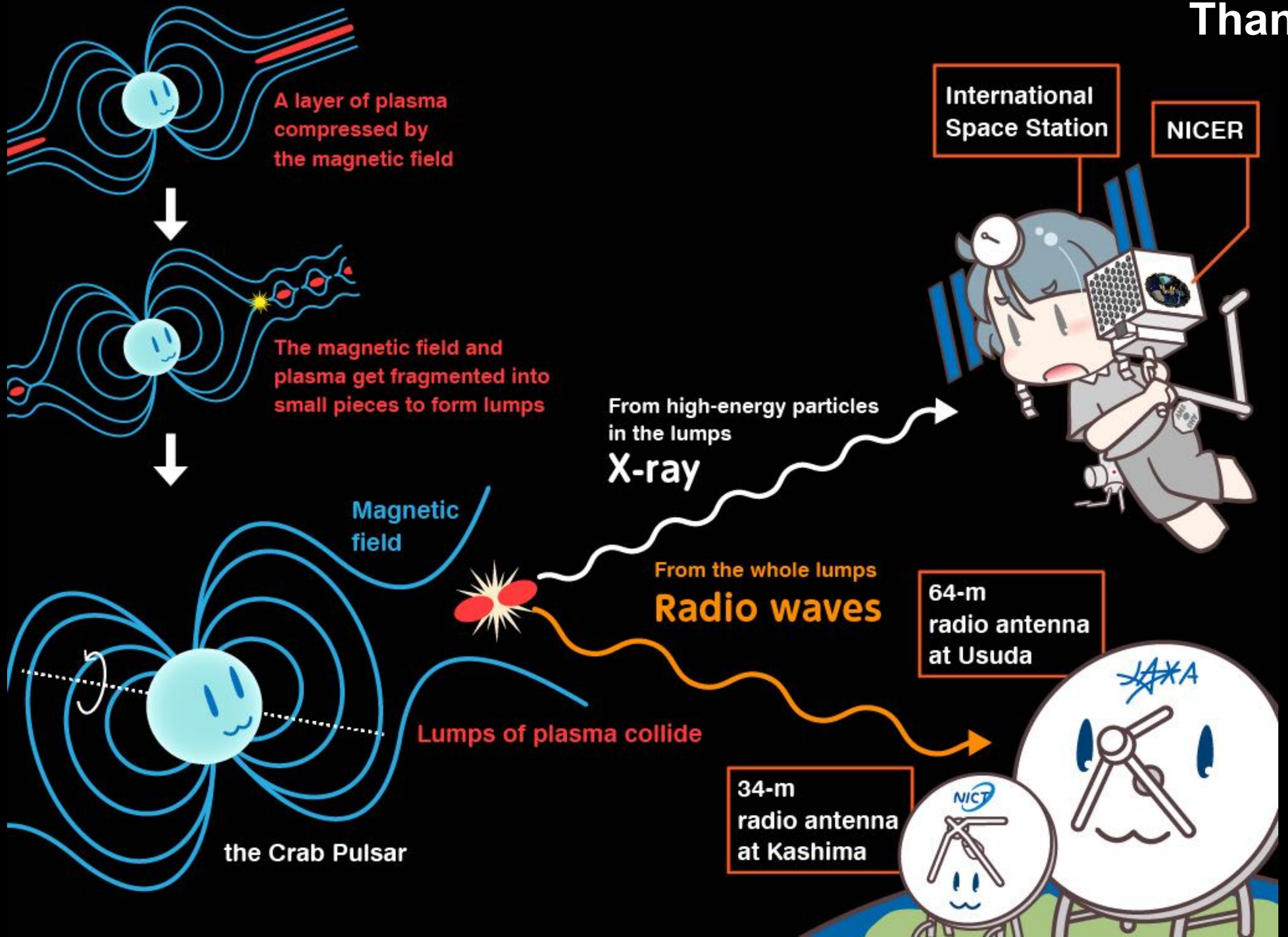

(Credig) Higgstan.com

おまけ: A new magnetar Swift J1555.2-5402

Open at arXiv yesterday: https://arxiv.org/abs/2108.02939

Astrophysics > High Energy Astrophysical Phenomena

[Submitted on 6 Aug 2021]

A month of monitoring the new magnetar Swift J1555.2-5402 during an X-ray outburst

Teruaki Enoto, Mason Ng, Chin-ping Hu, Tolga Guver, Gaurava K. Jaisawal, Brendan O'Connor, Ersin Gogus, Amy Lien, Shota Kisaka, Zorawar Wadiasingh, Walid A. Majid, Aaron B. Pearlman, Zaven Arzoumanian, Karishma Bansal, Harsha Blumer, Deepto Chakrabarty, Keith Gendreau, Wynn C. G. Ho, Chryssa Kouveliotou, Paul S. Ray, Tod E. Strohmayer, George Younes, David M. Palmer, Takanori Sakamoto, Takuya Akahori, Sujin Eie

The soft gamma-ray repeater Swift J1555.2-5402 was discovered by means of a 12-ms duration short burst detected with Swift BAT on 2021 June 3. Then 1.6 hours after the first burst detection, NICER started daily monitoring of this X-ray source for a month. The absorbed 2-10 keV flux stays nearly constant at around 4e-11 erg/s/cm2 during the monitoring timespan, showing only a slight gradual decline. A 3.86-s periodicity is detected, and the time derivative of this period is measured to be 3.05(7)e-11 s/s. The soft X-ray pulse shows a single sinusoidal shape with a root-mean-square pulsed fraction that increases as a function of energy from 15% at 1.5 keV to 39% at 7 keV. The equatorial surface magnetic field, characteristic age, and spin-down luminosity are derived under the dipole field approximation to be 3.5e+14 G, 2.0 kyr, and 2.1e+34 erg/s, respectively. An absorbed blackbody with a temperature of 1.1 keV approximates the soft X-ray spectrum. Assuming a source distance of 10 kpc, the peak X-ray luminosity is ~8.5e+35 erg/s in the 2--10 keV band. During the period of observations, we detect 5 and 37 short bursts with Swift/BAT and NICER, respectively. Based on these observational properties, especially the inferred strong magnetic field, this new source is classified as a magnetar. We also coordinated hard X-ray and radio observations with NuSTAR, DSN, and VERA. A hard X-ray power-law component that extends up to at least 40 keV is detected at 3-sigma significance. The 10-60 keV flux, which is dominated by the power-law component, is ~9e-12 erg/s/cm2 with a photon index of ~1.2. The pulsed fraction has a sharp cutoff above 10 keV, down to ~10% in the hard-tail component band. No radio pulsations are detected during the DSN nor VERA observations. We place 7{\sigma} upper limits of 0.043mJy and 0.026 mJy on the flux density at S-band and X-band, respectively.

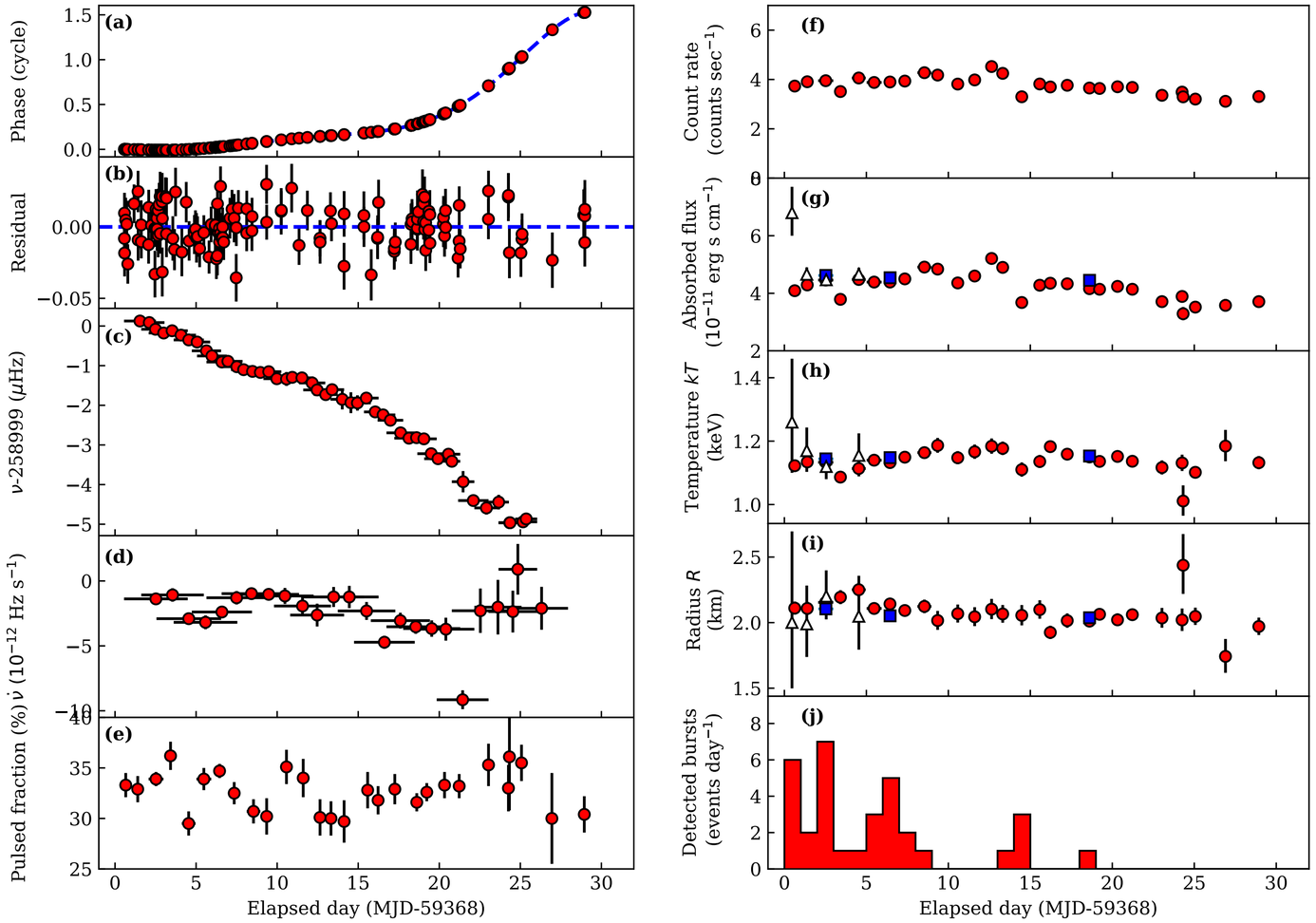

Figure 1. *NICER* monitoring of the timing (left panels) and spectral evolutions (right panels) of the 2021 outburst of Swift J1555.2−5402 over 29 days (2021 June 3–July 1; MJD 59368–59396). The time origin MJD 59368 is the day when the first burst was detected with *Swift*/BAT. (a) Intrinsic pulse-phase evolution with respect to a folding frequency of $\nu_{\rm fold} = 0.258997274$ Hz and a folding frequency derivative of $\dot{\nu}_{\rm fold} = -1.63 \times 10^{-12}$ Hz s^{-1}; dashed line is the best-fit model with a fifth-order polynomial. (b) Phase residuals (cycles) after correcting for the spin derivatives (up to 5th order). (c) Spin frequency with 2-day windows in steps of 0.5 days. (d) Spin frequency derivative with 4-day windows in steps of 1 day. (e) RMS pulsed fraction in the 3–8 keV band. (f) Background-subtracted 2–10 keV *NICER* count rate. (g) 2–10 keV absorbed X-ray flux obtained with *Swift* (open triangles), *NICER* only (red circles), and *NICER* simultaneously fitted with *NuSTAR* (blue squares). The symbols are the same in panels h and i. (h) Blackbody temperature (keV). (i) Emission radius of the blackbody component assuming a fiducial distance of 10 kpc. (j) Number of short bursts per day detected with *NICER* and *Swift*/BAT. Error bars are 68% confidence limit in these plots.

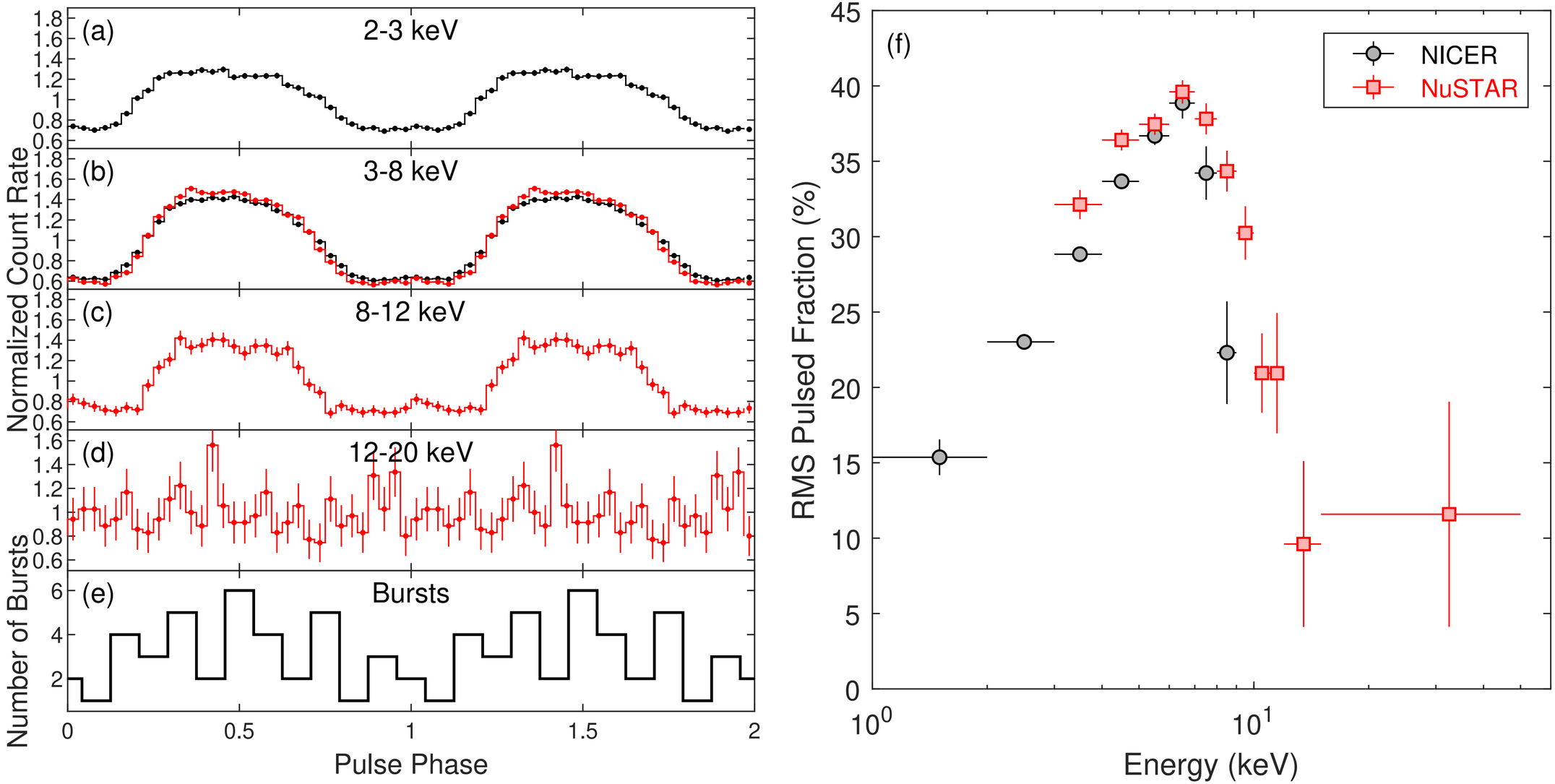

Figure 2. Left: Panels (a)–(d) are background subtracted X-ray pulse profiles of Swift J1555.2−5402 in the 2–3 keV, 3–8 keV, 8–12 keV, and 12–20 keV, respectively, taken with (black) *NICER* and (red) *NuSTAR*. The amplitudes are normalized relative to the mean count rate. Two cycles are shown in this figure for clarity. Error bars indicate 1σ uncertainties. Panel (e) shows the phase distribution of short bursts. Right: RMS pulsed fraction as a function of energy.

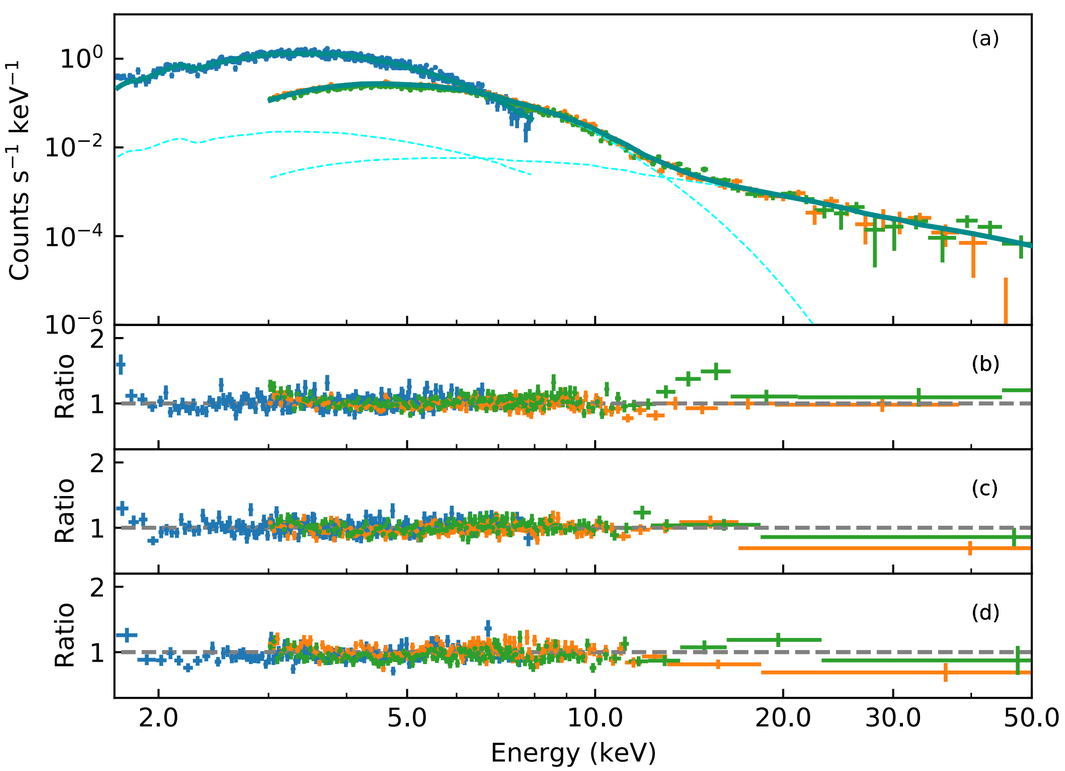

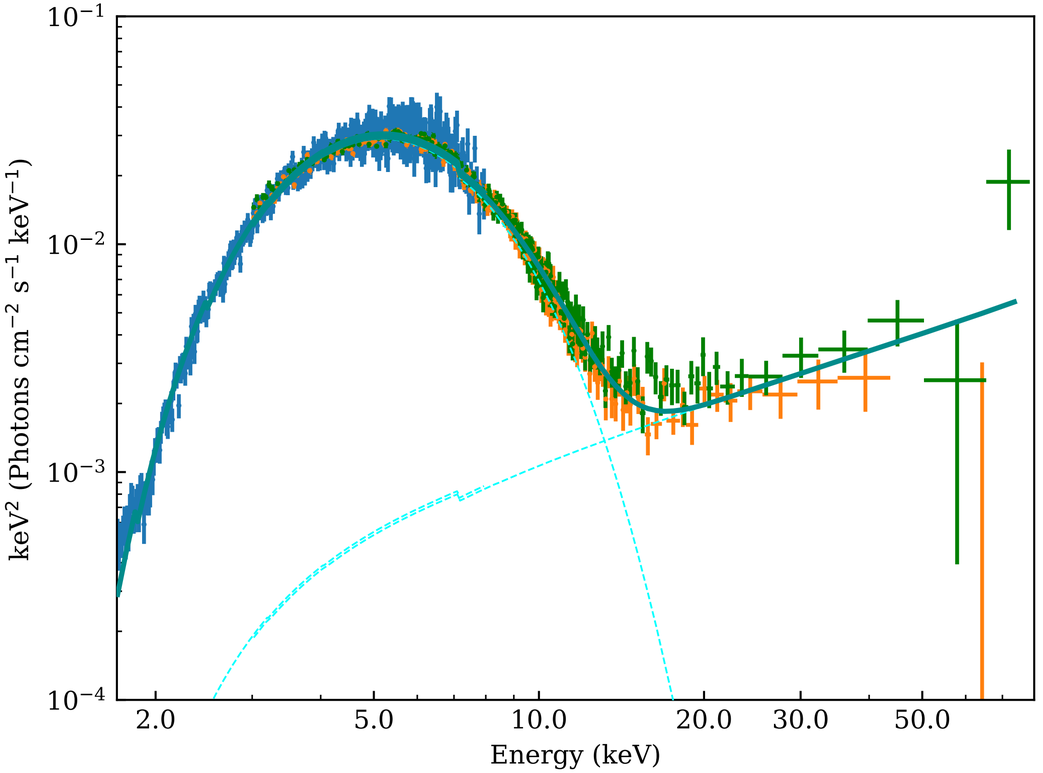

Figure 3. Left: Spectral fitting of the joint *NICER* and *NuSTAR* data of Swift J1555.2−5402. Panel (a) shows the background-subtracted response-inclusive spectra obtained on June 5 and the best-fit model (dark cyan solid line) with its blackbody and power-law components (cyan dashed lines). Photoelectric absorption is not corrected. Lower panels (b)-(d) show spectra obtained on June 5, 9, and 21, divided by the best-fit model to the first epoch shown in panel (a). Right: Best-fit νF_ν spectra of *NICER*, *NuSTAR* FPMA and FPMB for the three epochs combined. In both panels, *NICER* and *NuSTAR* FPMA and FPMB data are shown in blue, orange, and green, respectively.

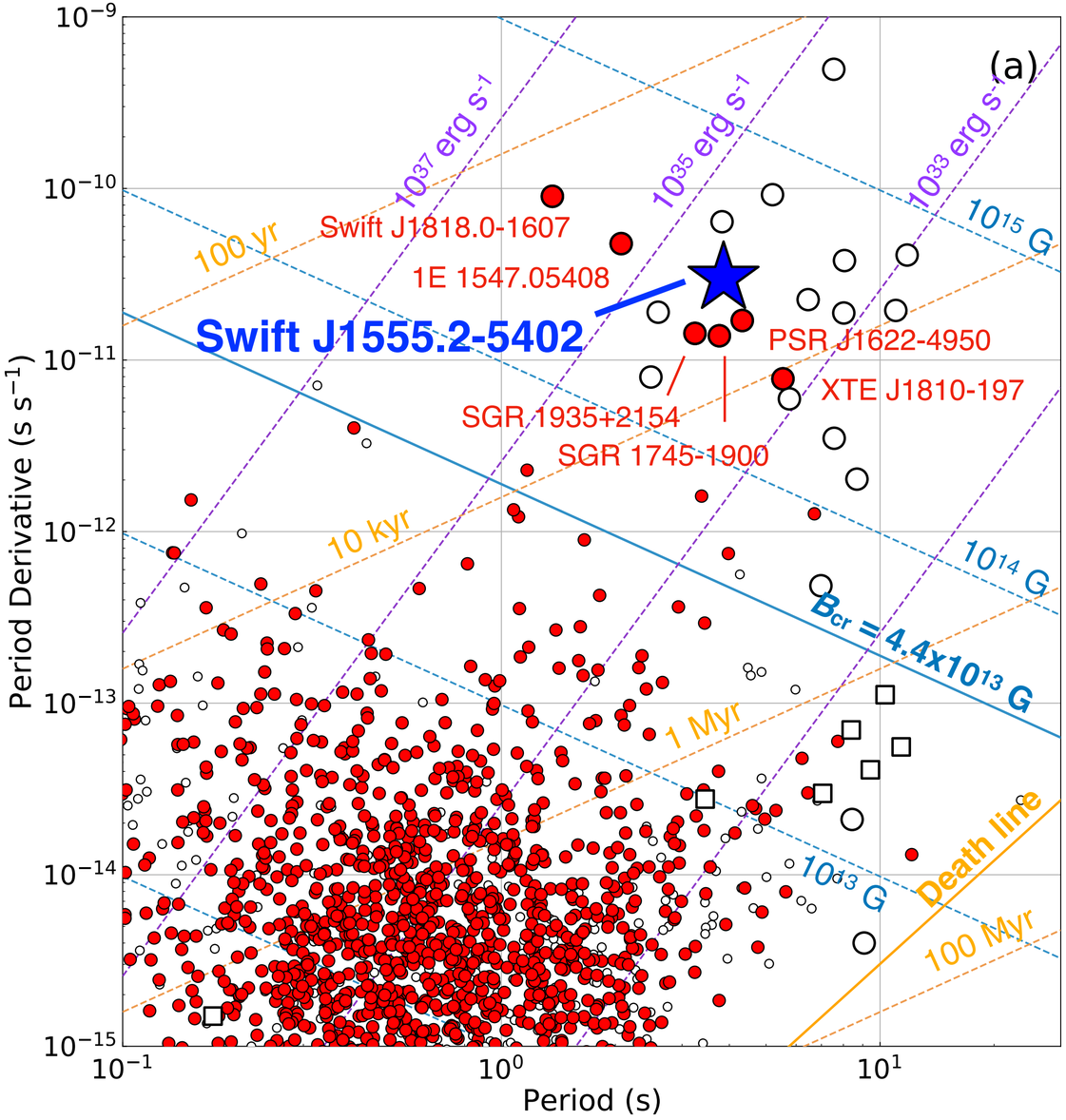
(a)
Swift J1818.0-1607
1E 1547.05408
Swift J1555.2-5402
PSR J1622-4950
XTE J1810-197
SGR 1935+2154
SGR 1745-1900
100 yr
10 kyr
1 Myr
100 Myr
Death line
10^{37} erg s^{-1}
10^{35} erg s^{-1}
10^{33} erg s^{-1}
10^{15} G
10^{14} G
10^{13} G
$B_{cr} = 4.4 \times 10^{13}$ G
Period Derivative (s s^{-1})
Period (s)

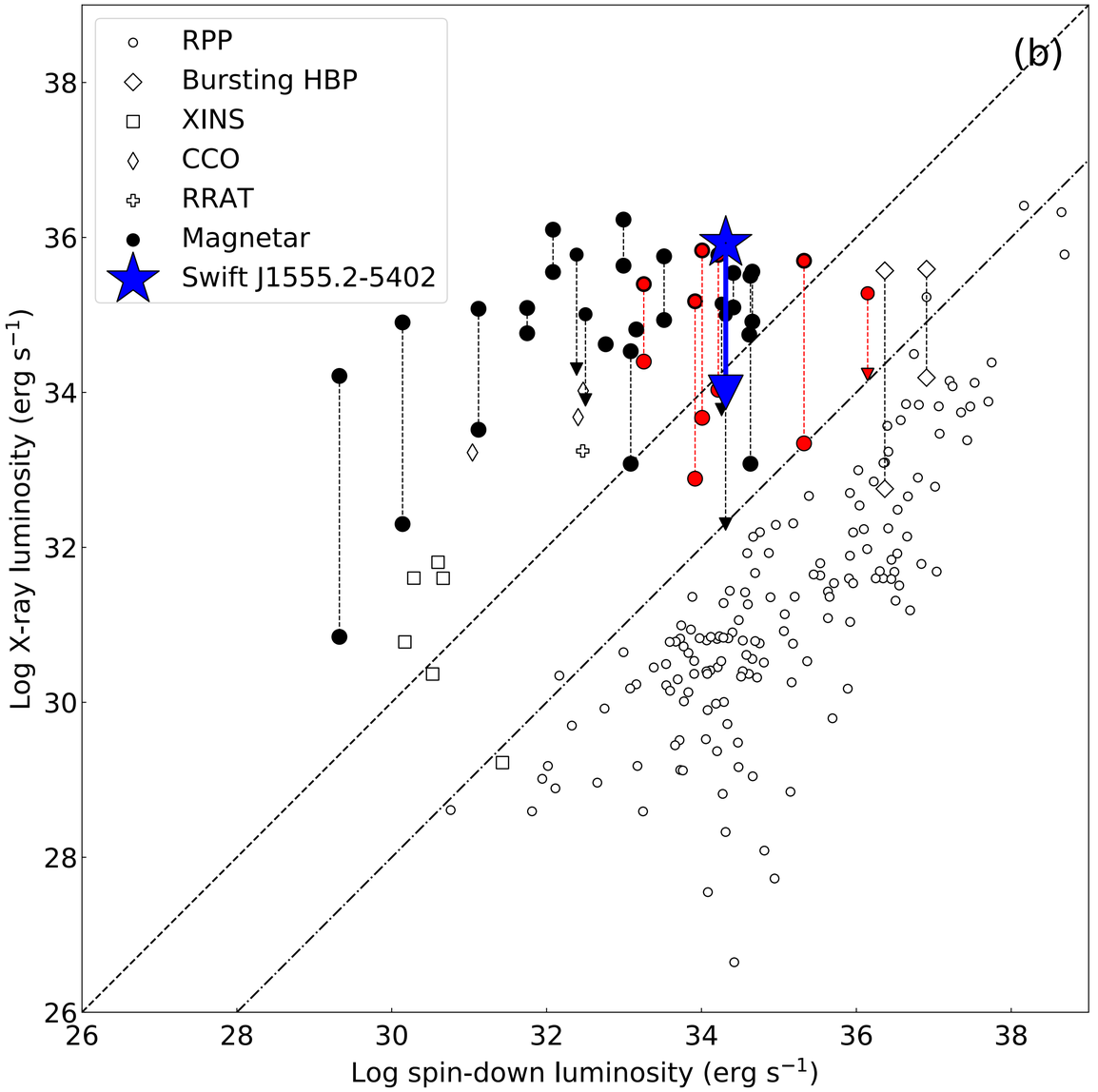
(b)
RPP
Bursting HBP
XINS
CCO
RRAT
Magnetar
Swift J1555.2-5402
Log X-ray luminosity (erg s^{-1})
Log spin-down luminosity (erg s^{-1})

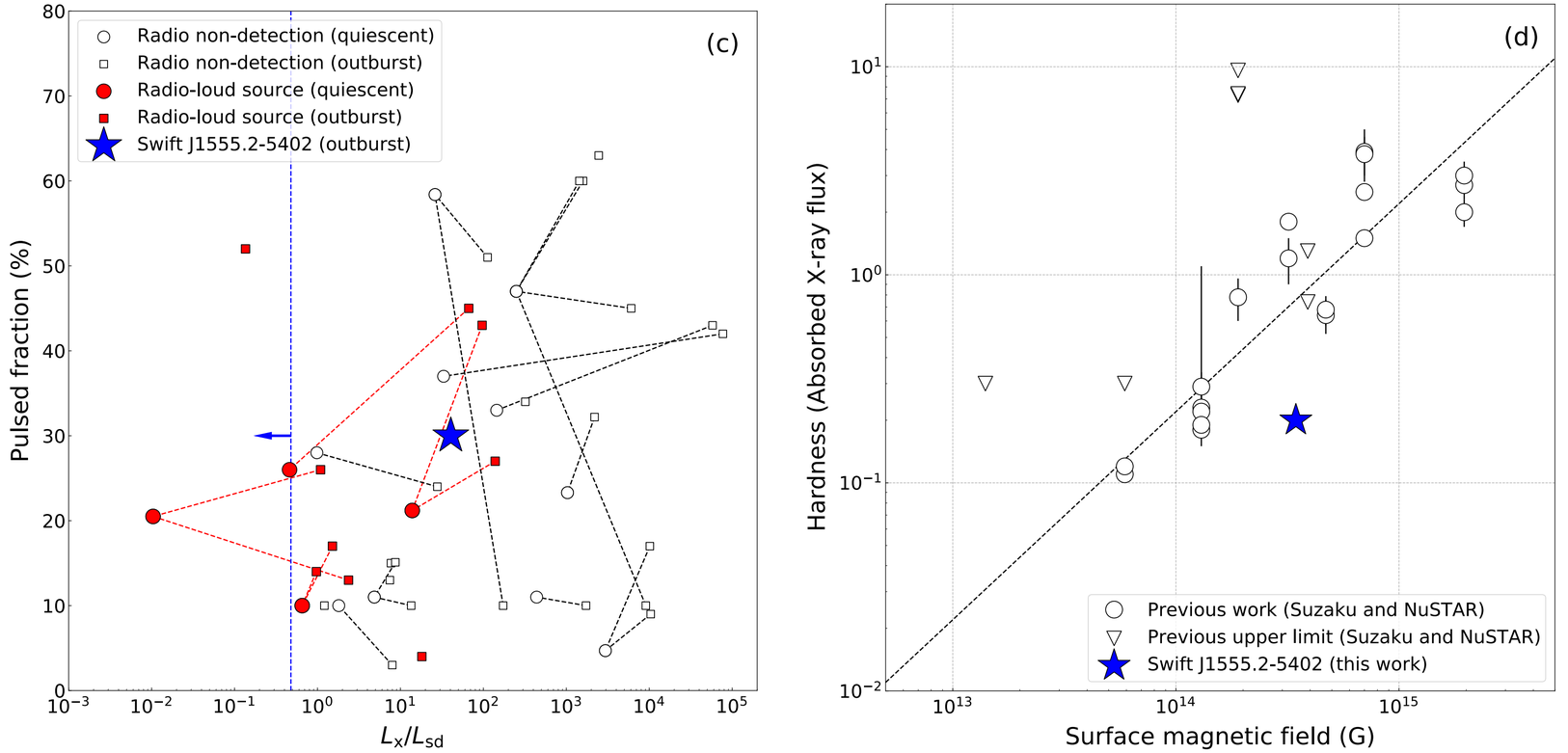

Figure 4. (a) Position of the new magnetar Swift J1555.2−5402 (star) on the P-$\dot{P}$ diagram. Large and small circles indicate magnetars (from the McGill catalog; Olausen & Kaspi 2014) and canonical rotation-powered pulsars (from the ATNF catalog; Manchester et al. 2005), respectively. Filled red symbols indicate radio-emitting pulsars. The lines show constant surface magnetic field strengths, characteristic ages, and spin-down luminosities. (b) Observed X-ray luminosity in the soft X-ray band (including the unpulsed component) compared with the spin-down power for various types of pulsars. The peak X-ray luminosity and quiescent values of magnetars are connected via dashed lines. Red symbols indicate radio-loud magnetars. The two diagonal lines indicate where the X-ray luminosity becomes equal to 100% and 1% of the spin-down power. The values and references used in panels (b)-(d) are summarized in Appendix Table D1 and D2 for magnetars and in Enoto et al. (2019) for other pulsars. (c) Pulsed fractions as a function of the X-ray luminosity normalized by the spin-down power. Filled red symbols indicate radio-emitting magnetars. Circles and squares represent data in quiescence and during X-ray outbursts, respectively. A dashed line connects observations for the same source. The vertical dashed line with the arrow indicates the region of the quiescent state of Swift J1555.2−5402. (d) The broad-band hardness ratio of absorbed X-ray fluxes between the 1–10 keV and 15–60 keV with the best-fit correlation (Enoto et al. 2017) .